Nucleotide sharing through gap junctions buffers replication stress

Benjamin Boumard[1], Gwenn Le Meur[1], Tania Maalouf[1], Marwa El-Hajj[1], Reinhard Bauer[2], Allison J. Bardin[1]*

[1] Institut Curie, PSL Research University, CNRS UMR 3215, INSERM U934, Stem Cells and Tissue Homeostasis Group, Paris, France.
[2] LIMES-Institute, Development, Genetics and Mol. Physiology Unit, Dpt. For Molecular Developmental Biology, University of Bonn, Carl-Troll-Str. 31,D-53115 Bonn

*Corresponding author. Email: allison.bardin@curie.fr

Cell proliferation underlying tissue growth and homeostasis, requires high levels of metabolites such as deoxynucleotides (dNTPs). The dNTP pool is known to be tightly cell-autonomously regulated through the *de novo* synthesis and salvage pathways. Here, we reveal that nucleotides can be provided to cells non-autonomously by surrounding cells of the tissue. *Drosophila* adult intestinal stem cells are highly sensitive to nucleotide depletion whereas wing progenitor cells are not. While adult intestinal stem cells lack gap junctions and their associated capacity to buffer dNTP pools, wing progenitor cells share nucleotides through connections to surrounding cells via gap junctions, allowing buffering of replication stress induced by nucleotide pool depletion. These findings have broad implications, suggesting that gap junction connectivity may define how sensitive cells are to changes in intracellular dNTP levels and replication stress.

Essential metabolic resources such as amino acids and nucleotides form the building blocks of cell growth and division. Deoxynucleotide (dNTP) production is tightly regulated and defects in dNTP balance can have dire effects, leading to replication stress, DNA damage, and high levels of genetic instability (*1-4*). dNTP production can occur via *de novo* synthesis and nucleotide salvage pathways. While *de novo* dNTP synthesis uses amino acids and folate cycle metabolites to produce dNTP, the salvage pathway relies on precursor deoxynucleosides (dNs) imported from the extracellular environment or recycled intracellularly from intermediate metabolites (*5*). Consistent with genetic phenotypes in mouse models inactivating *de novo* synthesis or salvage pathway components (*6-8*), proliferative tissues rely primarily on *de novo* dNTP synthesis (*4, 5, 9*).

A critical node of *de novo* synthesis is the enzymatic activity of ribonucleotide reductase (RNR), which catalyzes the rate limiting step of this pathway. It is exquisitely controlled with its activity peaking in S-phase when dNTPs are required, and being further allosterically tuned through binding of dNTPs (*10, 11*). In addition to this cell-intrinsic control of dNTP levels, external hormones and growth factors activate *de novo* dNTP synthesis, thereby linking local and systemic cues for tissue growth and cell proliferation to dNTP resource production (*12-15*). Thus, a large body of literature has demonstrated that dNTP levels are tightly regulated cell-autonomously with additional important input from extracellular signals leading to "privatized" cell-intrinsic production of dNTPs.

Here, we provide evidence of a novel mechanism by which dNTPs can be provided to a cell: collective resource sharing depending on exchange of nucleotides from neighboring cells through gap junctions. Our data indicate that this “socialized” mechanism acts within the developing wing disc allowing tissue-level regulation of nucleotides and can provide an important buffering mechanism when dNTP pools are perturbed. In contrast, adult intestinal stem cells (ISCs), which lack gap junctions, have privatized dNTP resources, and are incapable of buffering their dNTP pool when it is depleted. Thus, cells may “privatize” or “socialize” dNTP resources at the tissue-scale, which can impact their ability to respond to changes in dNTP levels. The ability to exchange dNTPs with neighboring cells has important implications for understanding the propensity of cells and tissues to acquire replication stress.

Previous data suggest a potential role for replication defects in promoting adult stem cell mutagenesis and age-related functional decline (*16-20*). We, therefore, further investigated how replication stress affects stem and progenitor cells using *Drosophila* adult intestinal stem cells and wing disc progenitor cells. Intestinal stem cells (ISCs) replenish terminally differentiated enteroendocrine cells (EEs) and enterocytes (ECs) during homeostasis and in response to tissue damage (Fig. 1A) (*21, 22*). To induce replication stress, we targeted the nucleotide pool through inactivation of *RnrL*, the large subunit of RNR, critical for dNTP synthesis (*11*). RnrL was found to be expressed in replication-competent cells in the intestine, with terminally differentiated cells lacking RnrL expression (fig. S1A-B, see also (*23*)). Knockdown (KD) of *RnrL* for 4 days in adult ISCs led to high levels of DNA damage with accumulation of γH2Av (the *Drosophila* ortholog of γH2Ax) and foci of Replication protein A (RpA70-GFP; Fig. 1B-E; fig. S1C-D). Consistent with induction of replication stress, an increased proportion of ISCs in S phase was detected by the FUCCI system (*24*) and higher levels of γH2Av in S phase than in G1 or G2 were observed (fig. S1E-H). Feeding adult flies with hydroxyurea (HU), a drug that inhibits RNR, also induced replication stress in ISCs as detected by γH2Av and RpA70-GFP (fig.S1I-L), and blocked stem cell proliferation (fig. S1M). Clonal inactivation of *RnrL* in ISCs and their lineage impacted clone growth and induced DNA damage in ISCs as well as other cells in the lineage, which rely on dNTPs for

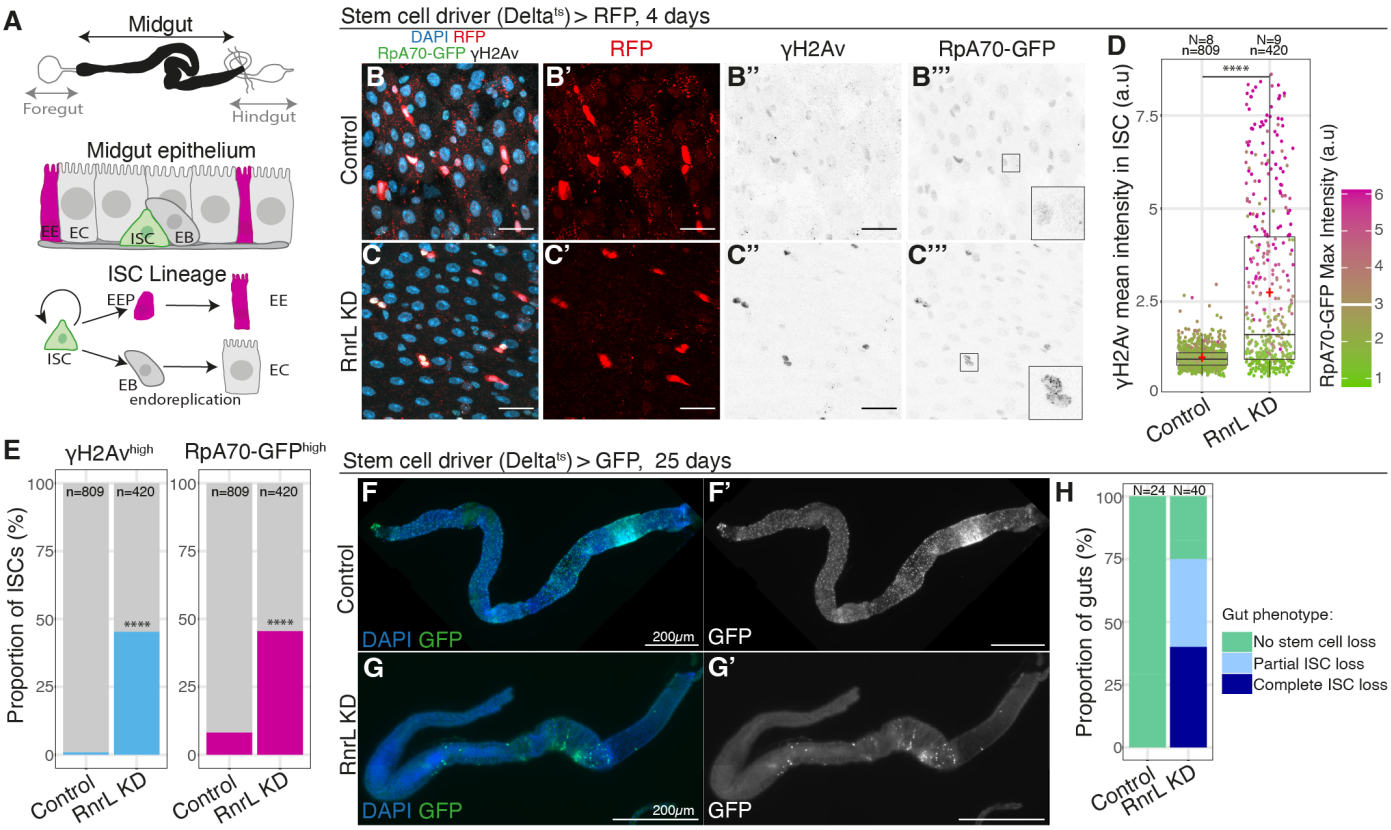

Figure 1. Midgut stem cells are sensitive to replication stress induced by RnrL inhibition.
A. Representation of the *Drosophila* digestive tract of which the midgut is the main compartment. The midgut epithelium and lineage are composed of Intestinal Stem Cells (ISCs), located basally, that can self-renew and produce Enterocytes (ECs) or Enteroendocrine cells (EEs) through Enteroblasts (EBs) progenitors or Enteroendocrine progenitors (EEPs). **B-C'''.** *Delta^{ts}>RFP, RpA70-GFP* female midguts without or with *RnrL* RNAi for 4 days, stained for DAPI, RFP, γH2Av, GFP. RFP and *RnrL* RNAi expression is specific to stem cells through the *Delta^{ts}* driver (*Delta-Gal4*, *tub-Gal80^{ts}*). Scale bar: 20µm. **D.** γH2Av mean intensity and RpA70-GFP max intensity in each ISC (RFP+) nuclei in Control or *RnrL* RNAi conditions, normalized to the mean value in the Control. The red crosses represent the mean value. Welch's t-test. **E.** Proportion of ISC (RFP+) with high levels of γH2Av (>2 of mean γH2Av intensity in D) or RpA70-GFP (>3 of max RpA70-GFP intensity in D). Fisher's test. **F-G'.** *Delta^{ts}>GFP* midguts aged for 25 days with or without *RnrL* RNAi. Stem cells were detected with GFP expression. Scale bar: 200µm **H.** Proportion of posterior midguts with normal phenotype or stem cell loss.
*: $p < 0.05$; **: $p < 0.01$; ***: $p < 0.001$; ****: $p < 0.0001$. N = number of guts quantified, n = number of cells quantified.

replication in S phase prior to terminal differentiation (fig. S2A-G). Both clonal KD as well as long-term depletion in ISCs of *RnrL* resulted in stem cell loss (Fig. 1F-H; fig. S2G). We conclude that the inactivation of *RnrL* in ISCs has strong effects, causing S phase delays, high levels of DNA damage, stem cell loss, and lineage perturbation. Our data indicate that intestinal stem cells are highly sensitive to replication stress induced by cell-autonomous nucleotide depletion, consistent with known reliance of proliferating cells on the cell intrinsic *de novo* pathway controlling dNTP production (*5*).

Surprisingly, we noticed that the progenitor cells of the developing wing imaginal disc, which undergo rapid proliferation during larval stages (Fig. 2A), behave differently upon nucleotide pool

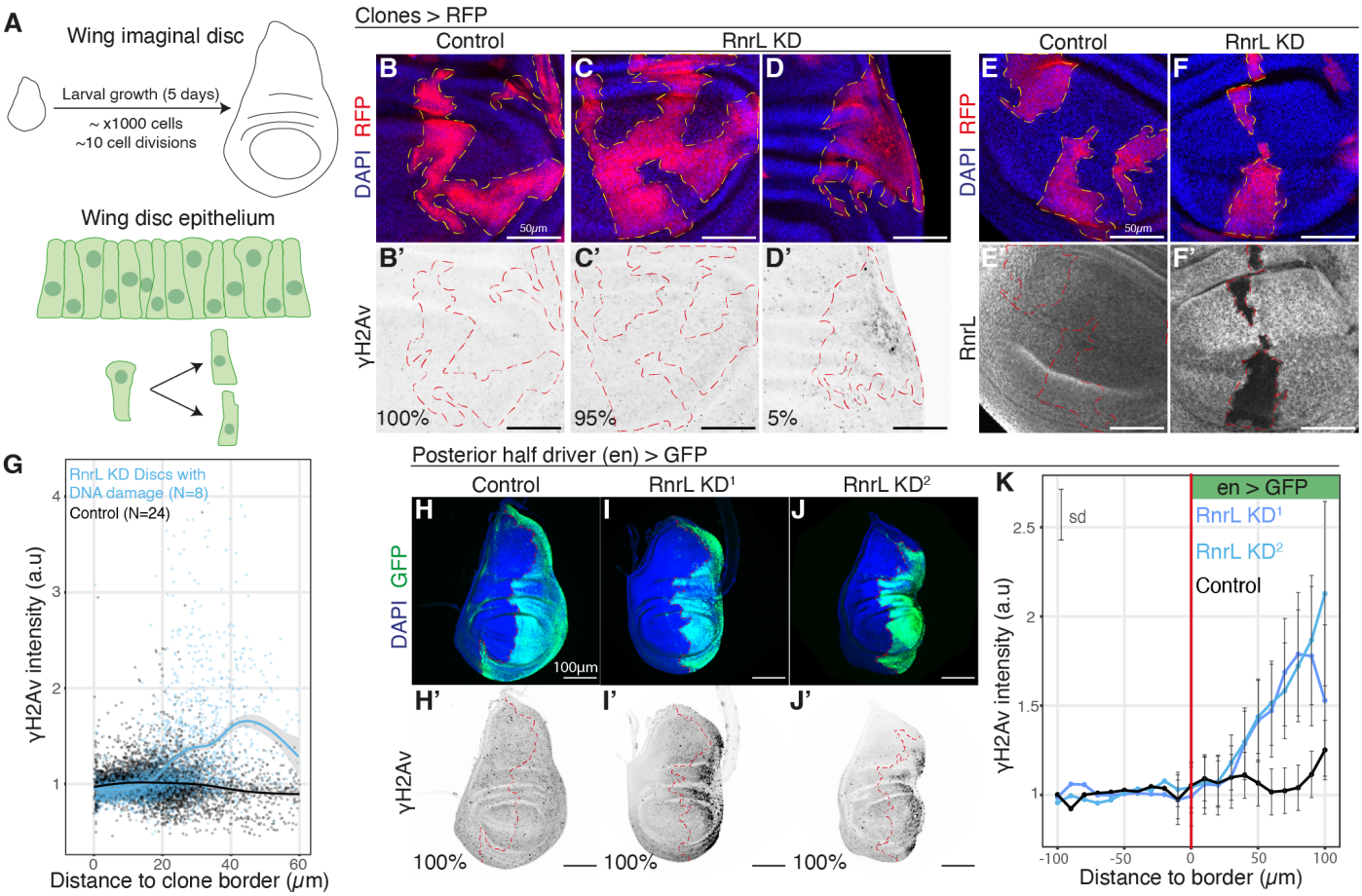

Figure 2. RnrL inhibition rarely induces DNA damage in the wing disc.
A. Representation of the *Drosophila* larval wing disc and wing disc epithelium. **B-D'.** hs-FlipOut>RFP clones in the late third instar larval wing disc, 4 days after induction in first instar larvae and stained for DAPI, RFP and γH2Av, with Control clones (B-B') and *RnrL* RNAi expressing clones (C-D'). ~95% of *RnrL* RNAi expressing clones had no detectible DNA damage (C-C'), whereas 5% of *RnrL* RNAi clones displayed a cluster of cells with higher levels of DNA damage at the center of the clone (D-D'). These wing discs and quantifications were obtained from the same experiment presented in Fig 3 A-F. Scale bar: 50µm. **E-F'.** hs-FlipOut> RFP clones in the late third instar larval wing disc, 4 days after induction in first instar larvae and stained for DAPI, RFP and RnrL. Control clones (E-E') showed homogenous RnrL staining similar to the surrounding wild-type tissue, while *RnrL* KD clones had lost RnrL throughout the clones (F-F'). Scale bar: 50µm. **G.** Mean γH2Av intensity per cells in the clones relative to the distance to the wild-type surrounding tissue (clone border), in *RnrL* RNAi discs that displayed DNA damage, and Control wild-type wing discs without DNA damage. For each condition, the line is the LOESS curve of local regression (y ~ x) from the represented dots and the gray area represents a 0.95 confidence interval. The value was normalized to the mean γH2Av intensity in wild-type non clonal tissue (outside of the clones) for each wing disc. DNA damage was found more than 20-35µm from the clone border. See individual discs in fig. S4. **H-J'.** *en>GFP* Control disc (H-H') or discs expressing two different *RnrL* RNAi constructs (I-J'). The discs were dissected at late third instar larval stage and stained for DAPI, GFP and γH2Av. The border of the *engrailed* domain (GFP +, posterior) is shown with a red line. Scale bar: 100µm. **K.** γH2Av intensity along the antero-posterior axis and relative to the engrailed domain border in Control and *RnrL* expressing wing discs. For each disc, the γH2Av level wass normalized to the level outside the *engrailed* domain and averaged on 10µm intervals. Bars show the standard deviation calculated for each 10µm interval (sd).

reduction. In striking contrast to ISCs, a majority of *RnrL* KD clones in the wing disc lacked DNA damage and were indistinguishable from wild-type clones (~95%, n=506/533), with only ~5% of clones (+/- 3%, n=27/533) having some detectable γH2Av (Fig. 2B-F). RnrL protein was found to be efficiently depleted by KD (Fig. 2E-F'), therefore, why does clonal perturbation of RNR activity have a minimal effect on proliferating wing disc cells? We first considered that activity of the dNTP salvage pathway may produce dNTP precursors, making the *de novo* synthesis pathway non-essential in this context. To test this possibility, we knocked down the *dnk* gene, encoding the sole Deoxyribonucleoside Kinase in *Drosophila*, an essential component of the salvage pathway (fig. S3A-E'). The combined reduction of salvage and *de novo* pathway activity (*dnk* KD + *RnrL* KD) was similar to *RnrL* KD, with a majority of clones having no DNA damage (fig. S3F-L). In addition, the KD of *dnk* alone in clones did not increase DNA damage, despite efficient depletion of Dnk by RNAi (fig. S3A-E'). Thus, we conclude that the salvage pathway does not have a major role in compensating dNTP precursors in absence of *de novo* synthesis.

If the salvage pathway does not compensate for *de novo* nucleotide synthesis, how might wing progenitors divide in absence of RNR activity? One clue came from the ~5% of *RnrL* KD clones with DNA damage: we noticed that cells with γH2Av were positioned in the center of the clones, 20-35μm from the border with wild-type cells (Fig. 2D, D', G and fig. S4A-F). Furthermore, when *RnrL* was depleted in the posterior half of the wing disc using the *engrailed-Gal4* driver (fig. S4G-H'), high levels of DNA damage were detected on the posterior-most side, ~40-50 μm from the engrailed domain border with wild-type tissue (Fig. 2H-K'). Thus, only when *RnrL* KD cells are far from wild-type cells, do they acquire marks of DNA damage. We therefore explored an alternative hypothesis that a non-autonomous rescue mechanism of nucleotides may arise from neighboring wild-type cells in the tissue.

Considering the relationship between the location of cells with DNA damage and the proximity to wild-type tissue, we reasoned that nucleotides might be transferred from wild-type cells to *RnrL* KD cells. Gap junctions, which can allow the passage of small metabolites and ions (<1 kDa), are formed by interactions of transmembrane hemichannels which join between adjacent cells and form pores (fig. S5A)(*25*). In *Drosophila*, gap junctions are made by eight Innexin protein forming homotypic or heterotypic complexes (*26*). Previous work suggested that the sugar, GDP-L-fucose (~580 Da), can be transferred between cells of the wing disc in a manner that relies on the gap junction component Inx2 (*27*). We therefore hypothesized a role for gap junctions in the non-autonomous rescue mechanism in wing disc progenitor cells that can buffer replication stress via transfer of nucleotides (~500 Da). Consistent with this notion and the high sensitivity of ISCs to dNTP depletion, we found that gap junction proteins are absent from ISCs and only detected at the membrane of older, mature EC cells in the intestine (figs. S6 and S7). In the wing disc, the gap junction protein, Inx2 was broadly expressed (fig. S5B, B') and reduced upon expression of *Inx2* RNAi (fig. S5C, C'). While *Inx2* RNAi alone did not induce DNA damage (Fig. 3D, D', F, fig. S5D), co-depletion of *RnrL* and *Inx2* led to high levels of γH2Av in the clonal tissue (91% of clones, n= 243/267, Fig. 3E-F, fig. S5D). Thus, upon concomitant loss of gap junctions and RNR activity, DNA damage is observed, independent of proximity to wild-type cells. In addition, co-depletion of *RnrL* and *Inx2* resulted in smaller clones than controls, consistent with cell proliferation impairment due to replication problems (Fig. 3E, E' and fig. S5E).

If nucleotide sharing occurs through gap junctions to neighboring tissue, then blocking gap junctions in cells adjacent to those depleted for nucleotides should induce DNA damage at the border of these populations of cells. To test this, twin-spot clones were produced whereby GFP+ clones expressing *RnrL* RNAi were induced adjacent to clones marked by loss of RFP that were homozygous for $Inx2^{A}$, a null allele. Control genotypes did not show DNA damage at the RFP-/GFP+ clone boundary (fig. S8A,B). Consistent with the above data in Fig. 2C, C', ~5.2% of discs with *RnrL* KD GFP+ clones adjacent to RFP- wild-type tissue had γH2Av accumulation in middle of the GFP+ clones (Fig. 3G-G''', Fig. 3I; fig. S8C-D). However, supporting the notion of the transfer of nucleotides from adjacent cells via gap junctions, most *RnrL* KD GFP+ clones with DNA

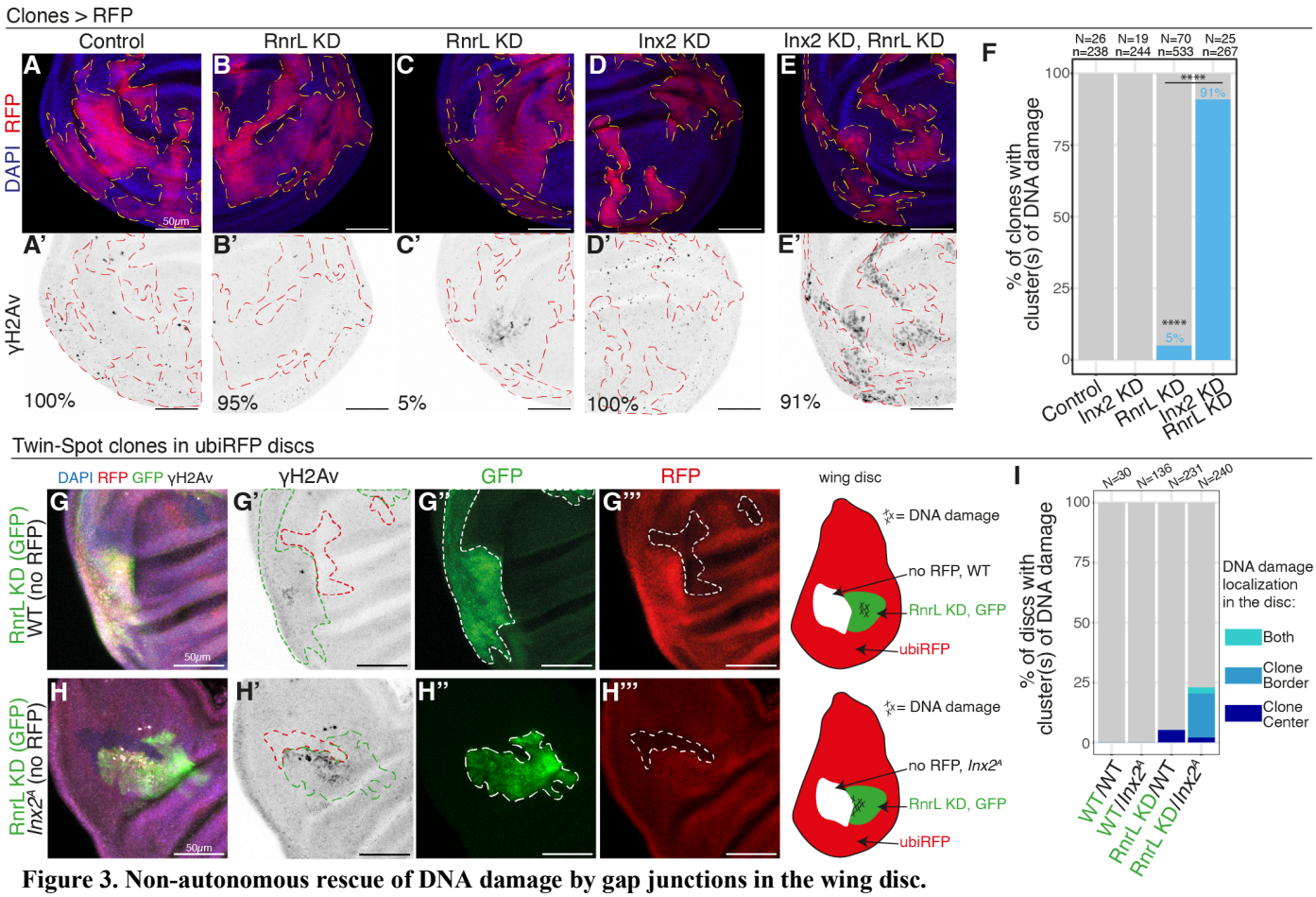

Figure 3. Non-autonomous rescue of DNA damage by gap junctions in the wing disc.
A-E'. hs-FlipOut>RFP clones in the late third instar larval wing disc, 4 days after induction in first instar larvae and stained for DAPI, RFP and γH2Av, with Control clones (A-A'), *RnrL* RNAi (B-C'), *Inx2* RNAi (D-D') and *RnrL&Inx2* RNAi (E-E'). Scale bar: 50µm. **F.** Proportion of clones with clusters of cells with DNA damage. Fisher's t-test. **G-H'''.** Twin spot clones in the wing disc with DNA damage (γH2Av), 4 days after induction in larvae and stained for DAPI, GFP, RFP and γH2Av. As indicated in the schematic, while the tissue expresses RFP ubiquitously, upon clone induction, one clone loses RFP expression and remains wild-type (WT; G-G''') or becomes *Inx2*^{A} homozygous mutant (H-H'''), and the twin clone gains Gal4/UAS driven expression of GFP and *RnrL* RNAi. See also Fig. S5 for additional twin-spot images. **I.** Percentage of discs with clones displaying clusters of cells with DNA damage (γH2Av), in discs γH2Av was either found at the center of the clone, at the border of the clone near *Inx2*^{A} clones or both. See also Fig. S8 for additional twin-spot images representing each category.
*: $p < 0.05$; **: $p < 0.01$; ***: $p < 0.001$; ****: $p < 0.0001$. N = discs.

damage had γH2Av accumulation at the border with RFP- *Inx2* mutant tissue (Fig. 3H-I; fig. S8E-H). These data support the model that gap junctions between cells buffer levels of nucleotides and replication stress.

Additional evidence for an important role of gap junctions in nucleotide sharing between wing disc cells was found upon knockdown of other enzymes important for dNTP synthesis upstream of RNR (fig. S9A). KD in the posterior compartment of the wing disc of *CTP-synthetase* (*CTPsyn*) and *Phosphoribosyl pyrophosphate synthetase* (*Prps*) alone did not result in DNA damage; however, the concomitant inactivation of gap junctions in these conditions showed γH2Av accumulation (Fig. 4A, B; fig. S9B). Similarly, the inactivation of GMP-synthetase, *bur*, resulted in gap junction-dependent appearance of DNA damage in 20% of discs (Fig. 3B, C; fig. S9A-B). A similar effect was observed upon KD of *dnk* (fig. S9D-G'). Of note, the knockdown of these nucleotides biosynthesis enzymes alone, did not result in DNA damage, unlike RnrL, which showed a gradient of DNA damage. This is consistent with RNR activity being a key rate-limiting step in dNTP production. Altogether, these data support gap junction-dependent buffering of nucleotide levels.

Finally, to provide direct evidence for gap junction-dependent nucleotide transfer, we took advantage of the fact that 5-ethynyl-2 deoxyuridine (EdU) is a nucleoside analogue that can be tracked in

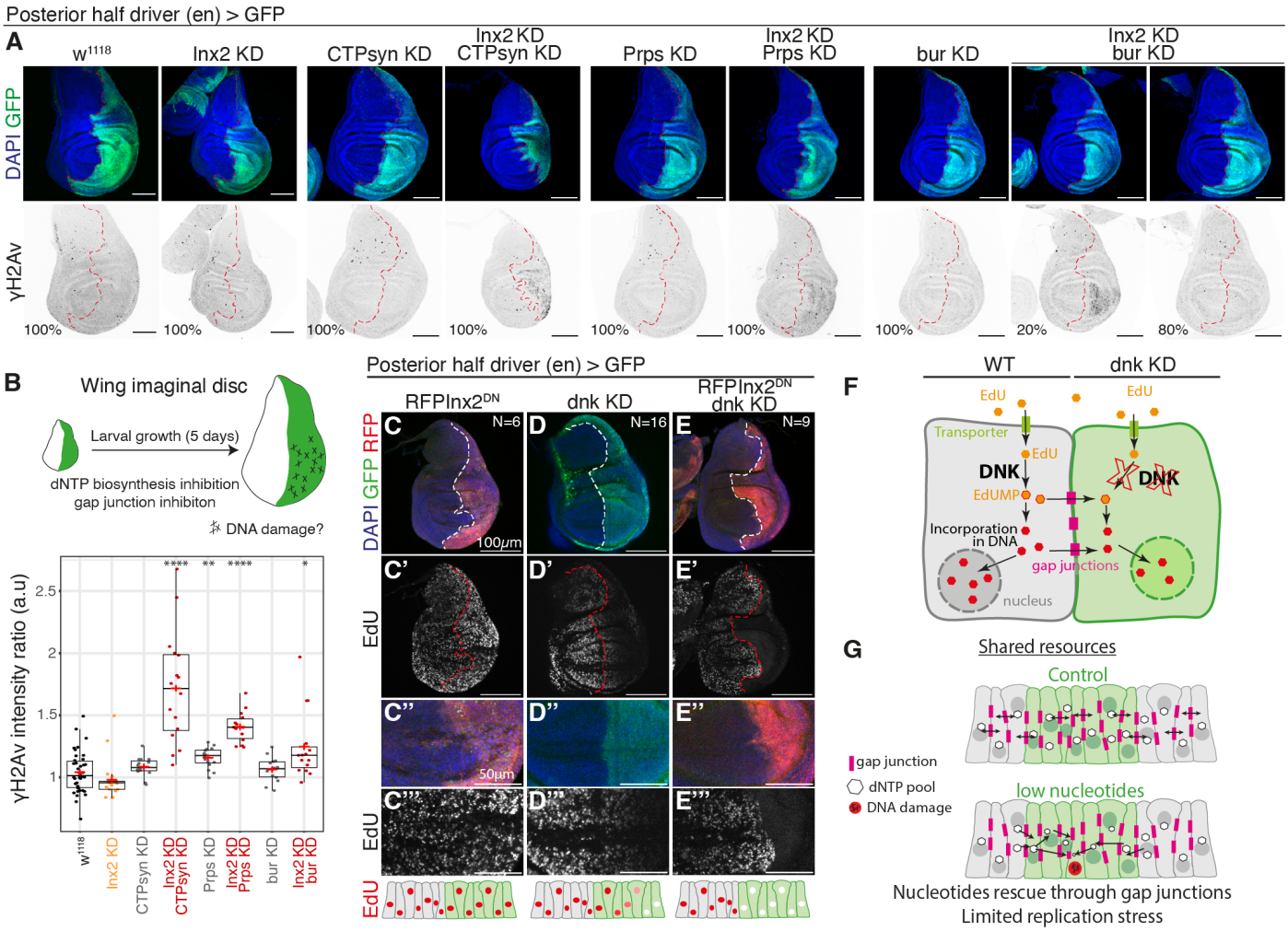

Figure 4. Nucleotide sharing through gap junctions in the wing disc epithelium.
A. *en>GFP* Control disc (w^{1118}), disc expressing *Inx2* RNAi, in combination with *CTP synthetase* RNAi, *Prps* RNAi or *bur* RNAi. The discs were dissected at late third instar larval stage and stained for GFP marking the domain of expression and γH2Av indicating DNA damage. Scale bar: 100µm. **B.** γH2Av mean intensity in the pouch region of the engrailed domain (posterior, GFP+) relative to the mean intensity in the pouch region of the non-engrailed domain (anterior, GFP-), for the conditions represented in E. Welch's t-test. **C-E'''.** *en>GFP* disc expressing a dominant negative form of Inx2 (RFPInx2^{DN}, C-C'''), *dnk* RNAi (D-D'''), or both (E-E''') labelled for EdU after 30 mins incorporation at the late L3 larval stage. Scale bar: 100µm. **F.** Model of EdU incorporation in DNA, phosphorylation by DNK is required to allow the incorporation of EdU. EdU nucleotides can be transferred through gap junctions and incorporated in the DNA of cells that lack *dnk* expression but are connected to WT cells. **G.** Model of nucleotide sharing through gap junctions in the wing disc epithelium, contributing to limiting replication stress and DNA damage.
*: $p < 0.05$; **: $p < 0.01$; ***: $p < 0.001$; ****: $p < 0.0001$. N = discs. Red cross = mean

the cell through fluorescent labelling. EdU is imported into the cell through nucleoside transporters and then converted via the salvage pathway (DNK) into EdU-monophosphate (Fig. 4F). *dnk*, therefore, is essential to produce an EdU form that can be incorporated into DNA during replication, and the KD of *dnk* should block EdU nuclear staining. However, if gap junctions transport dNTPs between neighboring cells, sharing of the EdU nucleotide produced in the adjacent wild-type cells with *dnk* depleted cells should occur, thus resulting in EdU nuclear incorporation in the adjacent *dnk* depleted cells (Fig. 4F). To test this, we assessed EdU *ex vivo* incorporation upon KD of *dnk* in the posterior compartment of the wing disc. While control discs expressing a dominant-negative form of Inx2 (RFP-Inx2^{DN}) incorporated EdU throughout anterior and posterior compartments, *dnk* KD resulted in a graded appearance of EdU nuclear labelling in the posterior compartment, indicating that EdU-triphosphate was present in these cells despite the lack of *dnk* required to produce it (Fig. 4C-D'''). The EdU nuclear labelling gradient was abolished upon gap

junction inhibition (Fig. 4E-E"'), indicating that gap junctions allow the passage between cells of nucleotides.

Altogether, these findings lead us to propose that the resource sharing of nucleotides through gap junctions provides a novel source of dNTPs which can buffer replication stress at the tissue-level (Fig. 4G). Moreover, these data suggest that the gap junction connectivity can impact how sensitive cells are to changes in intracellular dNTP and replication stress. These findings have important implications for our understanding of how cell-cell communication and resource sharing can affect cell division, susceptibility to mutation, and cancer initiation. Furthermore, this raises the possibility that cell- and tissue-specific differences in capacity to share nucleotides may elicit differential effects of antimetabolite chemotherapeutics.

References:

1. H. Techer, S. Koundrioukoff, A. Nicolas, M. Debatisse, The impact of replication stress on replication dynamics and DNA damage in vertebrate cells. Nat Rev Genet 18, 535-550 (2017).
2. R. Buj, K. M. Aird, Deoxyribonucleotide Triphosphate Metabolism in Cancer and Metabolic Disease. Front Endocrinol (Lausanne) 9, 177 (2018).
3. A. da Costa, D. Chowdhury, G. I. Shapiro, A. D. D'Andrea, P. A. Konstantinopoulos, Targeting replication stress in cancer therapy. Nat Rev Drug Discov 22, 38-58 (2023).
4. N. J. Mullen, P. K. Singh, Nucleotide metabolism: a pan-cancer metabolic dependency. Nature Reviews Cancer, (2023).
5. J. Zhu, C. B. Thompson, Metabolic regulation of cell growth and proliferation. Nat Rev Mol Cell Biol 20, 436-450 (2019).
6. G. Toy et al., Requirement for deoxycytidine kinase in T and B lymphocyte development. Proc Natl Acad Sci U S A 107, 5551-5556 (2010).
7. V. N. Dobrovolsky, T. Bucci, R. H. Heflich, J. Desjardins, F. C. Richardson, Mice deficient for cytosolic thymidine kinase gene develop fatal kidney disease. Mol Genet Metab 78, 1-10 (2003).
8. P. Tran et al., De novo dNTP production is essential for normal postnatal murine heart development. J Biol Chem 294, 15889-15897 (2019).
9. E. S. Ali, I. Ben-Sahra, Regulation of nucleotide metabolism in cancers and immune disorders. Trends Cell Biol, (2023).
10. B. Stillman, Deoxynucleoside triphosphate (dNTP) synthesis and destruction regulate the replication of both cell and virus genomes. Proc Natl Acad Sci U S A 110, 14120-14121 (2013).
11. P. Nordlund, P. Reichard, Ribonucleotide reductases. Annu Rev Biochem 75, 681-706 (2006).
12. A. M. Robitaille et al., Quantitative phosphoproteomics reveal mTORC1 activates de novo pyrimidine synthesis. Science 339, 1320-1323 (2013).
13. I. Ben-Sahra, J. J. Howell, J. M. Asara, B. D. Manning, Stimulation of de novo pyrimidine synthesis by growth signaling through mTOR and S6K1. Science 339, 1323-1328 (2013).
14. J. B. French et al., Spatial colocalization and functional link of purinosomes with mitochondria. Science 351, 733-737 (2016).
15. I. Ben-Sahra, G. Hoxhaj, S. J. H. Ricoult, J. M. Asara, B. D. Manning, mTORC1 induces purine synthesis through control of the mitochondrial tetrahydrofolate cycle. Science 351, 728-733 (2016).
16. N. Riddiford, K. Siudeja, M. van den Beek, B. Boumard, A. J. Bardin, Evolution and genomic signatures of spontaneous somatic mutation in Drosophila intestinal stem cells. Genome Res 31, 1419-1432 (2021).
17. K. Siudeja et al., Frequent Somatic Mutation in Adult Intestinal Stem Cells Drives Neoplasia and Genetic Mosaicism during Aging. Cell stem cell 17, 663-674 (2015).

18. S. Alvarez et al., Replication stress caused by low MCM expression limits fetal erythropoiesis and hematopoietic stem cell functionality. Nat Commun 6, 8548 (2015).
19. J. Flach et al., Replication stress is a potent driver of functional decline in ageing haematopoietic stem cells. Nature, (2014).
20. I. Beerman et al., Proliferation-dependent alterations of the DNA methylation landscape underlie hematopoietic stem cell aging. Cell stem cell 12, 413-425 (2013).
21. B. Boumard, A. J. Bardin, An amuse-bouche of stem cell regulation: Underlying principles and mechanisms from adult Drosophila intestinal stem cells. Curr Opin Cell Biol 73, 58-68 (2021).
22. I. Miguel-Aliaga, H. Jasper, B. Lemaitre, Anatomy and Physiology of the Digestive Tract of Drosophila melanogaster. Genetics 210, 357-396 (2018).
23. A. Arnaoutov et al., IRBIT Directs Differentiation of Intestinal Stem Cell Progeny to Maintain Tissue Homeostasis. iScience 23, 100954 (2020).
24. N. Zielke et al., Fly-FUCCI: A Versatile Tool for Studying Cell Proliferation in Complex Tissues. Cell Rep 7, 588-598 (2014).
25. J. Syrjanen, K. Michalski, T. Kawate, H. Furukawa, On the molecular nature of large-pore channels. J Mol Biol 433, 166994 (2021).
26. A. Sanchez, C. Castro, D. L. Flores, E. Gutierrez, P. Baldi, Gap Junction Channels of Innexins and Connexins: Relations and Computational Perspectives. Int J Mol Sci 20, (2019).
27. T. Ayukawa et al., Rescue of Notch signaling in cells incapable of GDP-L-fucose synthesis by gap junction transfer of GDP-L-fucose in Drosophila. Proceedings of the National Academy of Sciences of the United States of America 109, 15318-15323 (2012).
28. P. Speder, A. H. Brand, Gap junction proteins in the blood-brain barrier control nutrient-dependent reactivation of Drosophila neural stem cells. Dev Cell 30, 309-321 (2014).
29. M. Furriols, S. Bray, A model Notch response element detects Suppressor of Hairless-dependent molecular switch. Curr Biol 11, 60-64 (2001).
30. F. Bosveld et al., Mechanical control of morphogenesis by Fat/Dachsous/Four-jointed planar cell polarity pathway. Science 336, 724-727 (2012).
31. A. J. Bardin, C. N. Perdigoto, T. D. Southall, A. H. Brand, F. Schweisguth, Transcriptional control of stem cell maintenance in the Drosophila intestine. Development 137, 715-724 (2010).
32. V. Loubiere et al., Coordinate redeployment of PRC1 proteins suppresses tumor formation during Drosophila development. Nat Genet 48, 1436-1442 (2016).
33. K. Ostrowski, R. Bauer, M. Hoch, The Drosophila innexin 7 gap junction protein is required for development of the embryonic nervous system. Cell Commun Adhes 15, 155-167 (2008).
34. C. M. Smendziuk, A. Messenberg, A. W. Vogl, G. Tanentzapf, Bi-directional gap junction-mediated soma-germline communication is essential for spermatogenesis. Development 142, 2598-2609 (2015).
35. G. Ammer, R. M. Vieira, S. Fendl, A. Borst, Anatomical distribution and functional roles of electrical synapses in Drosophila. Curr Biol 32, 2022-2036 e2024 (2022).
36. W. Knecht, B. Munch-Petersen, J. Piskur, Polyclonal antibodies against the ultrafast multisubstrate deoxyribonucleoside kinase from Drosophila melanogaster. Adv Exp Med Biol 486, 263-266 (2000).
37. J. Schindelin et al., Fiji: an open-source platform for biological-image analysis. Nat Methods 9, 676-682 (2012).
38. D. R. Stirling et al., CellProfiler 4: improvements in speed, utility and usability. BMC Bioinformatics 22, 433 (2021).

Acknowledgments:

We would like to thank the members of the Bardin team, P.-A. Defossez, Y. Bellaiche, P. Leopold, R. Basto, K. Siudeja, and C. Desplan for feedback on the manuscript. We thank G. Ammer, A. Arnaoutov, G. Tanentzapf, A. Lalouette, P. Spéder for antibodies and *Drosophila* lines as well as the Bloomington and Vienna stock centers for fly lines. We thank Prof. M. Hoch for his support of innexin research at the Limes institute. Microscopy training and access has been provided by The Cell and Tissue Imaging Facility/UMR3215 (PICT-IBiSA) of the Institut Curie, members of the French National Research Infrastructure France-BioImaging, ANR10- INBS-04.

Funding:

Work in the Bardin lab is supported by Fondation pour la Recherche Médicale (A.J.B., EQ202003010251), the program "Investissements d'Avenir" launched by the French Government and implemented by ANR, ANR SoMuSeq-STEM (A.J.B., ANR-16-CE13-0012-01), ANR ChronoDamage (A.J.B., ANR-20-CE13-0013_01), Labex DEEP (ANR11-LBX-0044), IDEX PSL (ANR-10-IDEX-0001-02 PSL). Salary support for A.J.B. was from the CNRS and B.B from ENS Lyon, FRM (FDT202001010957). R.B was supported by the SFB 645.

Author Contributions:

Conceptualization: BB, AJB.

Methodology: BB, AJB.

Reagent contribution: RB.

Investigation: BB, GLM, TM, ME-H,

Visualization: BB, AJB

Funding acquisition: BB, AJB.

Project administration: AJB.

Supervision: BB, AJB.

Writing – original draft: BB, AJB.

Writing – review & editing: BB, RB, AJB.

Competing interests: Authors declare that they have no competing interests.

Data and materials availability: All data are available in the main text or the supplementary materials, and all reagents can be made available from the corresponding author upon request.

MATERIALS AND METHODS

Fly Stocks

The experiments presented in this manuscript used the following fly lines.

From the Bloomington stock center: *UAS-2XGFP* (BL6874), *UAS-nlsRFP* (BL30556), *UAS-RnrL RNAi* #1 (BL51418), *UAS-RnrL RNA*i #2 (BL44022), CTPsyn RNAi #1 (BL53378), UAS-CTPsyn RNAi #2 (BL31752), UAS- UAS-CTPsyn RNAi #3 (BL31924), UAS-Prps RNAi #1 (BL60086), UAS-Prps RNAi #2 (BL35219), UAS-dnk RNAi #3 (BL65886), UAS-dnk RNAi #4 (BL35219), UAS-bur RNAi #1 (BL60432), UAS-bur RNAi #2 (BL31055), *Inx2^{A} FRT19A* (BL54481), From the Vienna Drosophila Resource Center: UAS-dnk RNAi #1 (v39137), UAS-dnk RNAi #2 (v103385).

The following stocks were gifts: *w^{1118}* (M. McVey); *RpA70-GFP* (*24*) (E. Wieschaus); FUCCI (*24*)(B. Edgar); *En-Gal4* (Y. Bellaiche, P. Leopold); *UAS-Inx2RNAi and UAS-RFPInx2^{DN}* (*28*)(P. Spéder); Su(H)GBE-LacZ (*29*) (S. Bray); *MARCM19A* and *FRT19A* (A.Gould); hs-flp; ; *tub-FRT-GAL80-FRT-GAL4*, *UAS-mRFP/TM6b, Tb, Hu* (originally gift of E. Martin-Blanco to Y. Bellaiche; (*30*)).

The *Delta^{ts}* line was generated from the *DeltaGal4/TM6TbHu* (S. Hou). It was used to generate: *UAS-2xGFP; Delta^{ts}/ TM6TbHu*; *UAS-RFP;Delta^{ts}/ TM6TbHu*; *FUCCI; Delta^{ts}/TM6TbHu.*

The flies used for the TwinSpot experiment were generated using stocks from the Bloomington stock center: BL42726, BL31406, BL54481, BL51418

The table S1 summarizes all the stocks used, and the table S2 indicates the genotypes used and represented in each figure.

Unless indicated the flies were kept at 25°C on standard medium with yeast. For the temperature sensitive experiments, flies were crossed at 18°C and the progeny kept at 18°C until 2-3 days old adult were collected and transferred at 29°C for the time of the experiment (2, 4, 8 or 25 days) before dissection, with fresh medium provided every 2-3 days.

HU feeding

For the hydroxyurea (HU, Sigma-Aldrich H8627) feeding experiments, 3-4 days old flies were placed on food supplemented with sterile distilled water (Control) or 10 mg/mL of HU diluted in sterile distilled water.

Clone Induction

MARCM in the gut: For the clone induction in the gut, adult flies 2-3 days after eclosion were heat-shocked at 36.5°C for 30 mins and then kept at 25°C on yeasted food for the duration of the experiment.

FlipOut and TwinSpots in wing disc:

For the clone induction in the larval wing discs, adult flies were left on yeasted food at 25°C to lay eggs for 24 hours. Progenies were heat-shocked at 37°C for 1h, 24 hours after the end of the egg laying period, and then kept at 25°C for the duration of the experiment. The wing discs were dissected 90-96 hours later, at late L3 stage (wandering larvae).

Immunostaining

Guts:

The tissues were fixed and stained following a previously published protocol (*31*). Briefly, the flies were dissected in Dulbecco's PBS (Sigma-Aldrich D1408) and the tissues were fixed at room temperature in 4% paraformaldehyde for 2 hrs (female guts). They were then washed in PBS + 0.1% Triton X-100 (Euromedex 2000-C) (PBT). To remove the content of the gut lumen, the fixed guts were equilibrated 30 mins in PBS-50% Glycerol (Sigma-Aldrich G9012) and then washed in PBT to osmotically release gut contents. The primary antibody staining was performed overnight at 4°C in PBT. After washing with PBT 20 mins, 3 times, the secondary antibodies were incubated 3-4 hrs at room temperature (RT). After washing with PBT 2 times, nuclei were counterstained with DAPI in PBT for 20 mins (1µg/ml).

Discs:

Adapted from a protocol provided by V. Loubiere ((*32*) G. Cavalli lab). Wandering larvae were collected, and wing imaginal discs were quickly dissected at RT in 1× PBS before being fixed for 20 min in 4% paraformaldehyde. Imaginal discs were then permeabilized for 1 hour in 1× PBS + 0.5% Triton X-100 and blocked for 1 hour in 3% bovine serum albumin (BSA) PBTr (1× PBS + 0.025% Triton X-100). Then, primary antibodies were added in 1% BSA PBTr and incubated overnight at

4°C. The following day, discs were washed in PBTr, secondary antibodies were added and incubated for 2 hours at RT. After washing with PBTr, nuclei were counterstained with DAPI in PBTr for 20 mins (1µg/ml).

Antibodies: The antibodies used were: chicken anti-GFP (1:2000, Invitrogen #A10262), rabbit anti-DsRed (1:1000, Clontech #632496), mouse anti-RFP (Invitrogen (RF5R), rabbit anti-γH2Av (1:2000, Rockland 600-401-91), , rabbit anti-Inx7 (*33*) (1:100, R. Bauer), guinea pig anti-Inx2 (*34*) (1:1000, G. Tanentzapf), rabbit anti-Inx2 (*35*) (1:1000, G. Ammer), rabbit anti-Inx3 (*35*) (1:70, R. Bauer), goat anti-βGal (1:200, F. Schweisguth), chicken anti-βGal (1:2000, Abcam ab9361), rabbit anti-PH3 (ser10, 1:2000, Merck Millipore #06-570), rabbit anti-RnrL (*23*) (1:200, A. Arnaoutov), rabbit anti-DNK (*36*)(1:20000, A. Lalouette). Also listed in table S3.

The antibodies mouse anti-γH2Av (1:200, DSHB UNC93-5.2.1), mouse anti-Delta (1:1000, DSHB C594.9B), mouse anti-Arm (1:200, DSHB N2 7A1), mouse anti-Pros (1:2000, DSHB MR1A-c), and mouse anti-Cora (1:100, DSHB C615.16) were developed respectively by R. S. Hawley (Stowers Institute), S. Artavanis-Tsakonas (Harvard Medical School), E. Wieschaus (Princeton University), C.Q Doe (University of Oregon), and R. Fehon (University of Chicago), and were obtained from the Developmental Studies Hybridoma Bank, created by the NICHD of the NIH and maintained at The University of Iowa, Department of Biology, Iowa City, IA 52242.

The secondary antibodies were all from Jackson Laboratory, raised in donkey with different fluorophores (DyLight 488, 549, 649), see table S3 for reference.

5-ethynyl-2 deoxyuridine (EdU) treatment and labelling

For the EdU incorporation experiment, wandering larvae (late L3 stage) were collected and dissected in Schneider's culture medium supplemented with L-glutamine (Sigma-Aldrich S0146) for 10mins. Then, EdU (Invitrogen by Thermo Fisher Scientific - C10340) was added to the dissection medium at a final concentration of 1µM, and the dissected wing discs were incubated for 30 mins at 25°C. After washing once quickly with PBS, the wing discs were fixed with PFA and stained with different antibodies following the procedure detailed above. The EdU Click-iT™ reaction was then performed for 30 mins following the manufacturer's protocol to label incorporated EdU with Alexa Fluor™ 647 dye (Invitrogen by Thermo Fisher Scientific - C10340). After washing with PBTr, nuclei were counterstained with DAPI in PBTr for 20 mins (1µg/ml).

Microscopy and Image Analysis

Pictures showed here were taken at the Cell and Tissue Imaging Platform – PICT-IBiSA of the UMR3215 of Institut Curie using the Zeiss confocal microscope LSM900 with a water 25x objective (whole discs), oil 40x objective (most of the gut images), Zeiss confocal microscope LSM780 with oil 25x objective (whole-disc images); Zeiss Apotome microscope 10X (whole-gut images). The images were processed, and the quantification performed using Fiji, unless another software is mentioned below.

PH3+ cells, stem cell loss and MARCM clone size:

For visualizations and quantifications of stem cell loss, MARCM clone size (cell number per clones) and PH3+ cells in adult midguts, we used a 20x dry objective on the Leica epifluorescence microscope DM6000B to score each phenotype.

FUCCI and MARCM analysis in the gut:

For the quantifications of FUCCI and clonal (MARCM) experiments in the gut, we used Fiji/ImageJ (*37*) for microscope image processing and quantifications. Cell nuclei were manually outlined on Fiji for γH2Av intensity measures.

For the FUCCI experiment, GFP and RFP intensities were also measured in the outlined nuclei, the ratio of GFP and RFP intensity and a visual confirmation allowed the attribution of cell cycle phases to individual stem cells.

For the clonal (MARCM) experiments, the cells were attributed a specific identity based on Prospero, Delta and DAPI staining. ISC were identified with Delta staining, EEs with nuclear Prospero staining, ECs with a large nucleus (>20µm^2), and EBs had small nuclei (<20µm^2) without Delta or Pros. The

limit of 20µm^2 area for an EC nucleus was determined based on GFP staining in MyoAGal4 flies, in which GFP expression is driven specifically in ECs.

γH2Av mean intensity and RpA70-GFP max intensity measures in ISCs:

For the measure of γH2Av mean intensity and RpA70-GFP max intensity in ISCs, in the case of Delta^{ts} driven GFP or RFP expression: The detection and outline of ISC nuclei was performed automatically on Fiji from maximum projection of the confocal Z-stacks images with a simple macro that we implemented. Simply, the DAPI and GFP intensity were used, respectively, to automatically outline the cell nuclei and the ISC cell area. The intersection of both "masks" indicated stem cell nuclei. The intensity thresholds used for both channels were determined for each experiment as the value depends on varying staining conditions and microscope settings. Several rounds of smoothing on Fiji allowed the refinement of ISC nuclei outlines. Importantly, for the analysis, nuclei with area <5µm^2 or >20µm^2 (ECs or nuclei fusion due to the maximum projection) were not considered as they likely do not represent stem cells. From each outlined nuclei, we collected the mean γH2Av intensity and the maximum RpA70-GFP intensity, corresponding to the brightest foci in each nucleus. The data were then normalized to the mean value obtained in the Control conditions for each experimental replicate. The pictures for which the identification of stem cell nuclei was difficult (too much nuclei fusion in the maximum projection, or bad signal for DAPI or GFP) were discarded from the analysis.

RedFlipout clones γH2Av distance analysis:

We used CellProfiler ((*38*), www.cellprofiler.org) for the analysis of γH2Av intensity in the FlipOut clones in the wing discs. The CellProfiler analysis allows the semi-automatic detection with manual validation and correction of disc area based on DAPI intensity, and clone area based on RFP expression. From this, we measured the mean intensity in clonal (RFP+ DAPI+) and wild-type non-clonal (RFP- DAPI+) area for each wing disc analyzed. For each wing disc, CellProfiler also determined the approximate cell localization and nucleus area for single cells in the clones based on DAPI staining. For each identified cell, we extracted the position, γH2Av mean intensity in the area outlined and the shortest distance to the border of the clone (i.e. wild-type non-clonal tissue). The γH2Av intensity was then normalized to the mean γH2Av intensity found in the wild-type non-clonal area of the same wing disc, used as a baseline. Altogether it enabled the analysis of the relationship between DNA damage (γH2Av intensity) and the distance to the clone border. For each disc, we also measured the maximum distance of the identified cells in the RFP+ clone to the non-clonal part of the disc, as a proxy for the size of the clone.

Engrailed γH2Av measurements:

In the experiment with *RnrL* RNAi with the *engrailed-Gal4* (*en-Gal4*) driver, both GFP and γH2Av intensity were measured along the antero-posterior line of the wing disc. The GFP intensity was used to determine the border of the engrailed domain for each measure. For all the other experiments with *en-Gal4* driver, the mean γH2Av intensity was measured in an area of the pouch region of the engrailed domain (containing most of it) and compared with a similar area on the opposite side of the same wing disc, giving a "γH2Av intensity ratio" for each wing disc.

Twin-Spots:

For the Twin-Spot experiment, the wing discs were analyzed and imaged at the LSM780 Zeiss confocal microscope, images of all the discs with DNA damage were taken, and representative images of all phenotypes were also taken.

RnrL, Inx2, and Inx7 quantification in the gut:

For the RnrL, Inx2 or Inx7 quantification in the midgut, the cell types were identified based on Su(H)GBE-LacZ expression, Armadillo, Prospero, and DAPI staining (nuclear size). EB have a small nucleus and are βGal+ with a strong Armadillo (Arm) membrane staining, EEs were Pros+, young EC had a big nucleus (polyploid) and were also BGal+, the other ECs had a big nucleus and low Arm staining. ISC were identified with strong Arm membrane staining, basal localization, and absence of βGal. If a few puncta of Inx2 or Inx7 were found at the membrane of the identified cells, these were

considered with partial Inx2 or Inx7 localization at the membrane.

Data Processing and Statistics

Data Analysis was performed on Excel, Prism (version 9.0.1) or R (version 4.2.2) using the Rstudio interface (version 2022.07.02) and ggplot2 package (version 3.4.0). Initial training for the use of the ggplot2 package for data visualization was obtained by the U900 Bioinformatics unit of the Curie Institute. As indicated in the figures, the statistical significance was represented as follows: *: $p < 0.05$; **: $p < 0.01$; ***: $p < 0.001$; ****: $p < 0.0001$.

Supplementary Figures and Legends:

Figs. S1 to S9

Tables S1 to S3

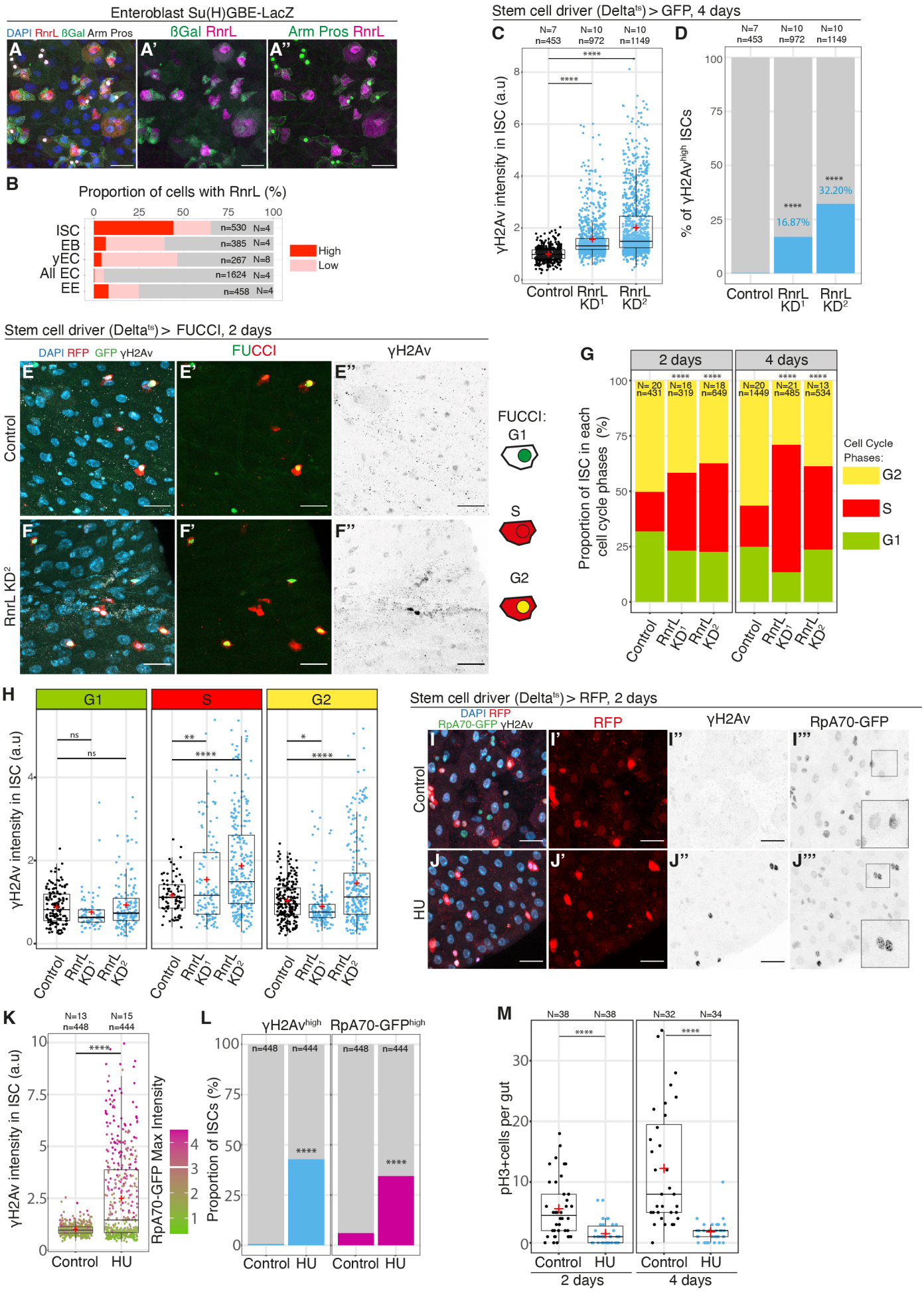
Enteroblast Su(H)GBE-LacZ
DAPI RnrL ßGal Arm Pros
ßGal RnrL
Arm Pros RnrL
A
A'
A''
B
Proportion of cells with RnrL (%)
ISC
EB
yEC
All EC
EE
High
Low
Stem cell driver (Delta^ts) > GFP, 4 days
C
D
γH2Av intensity in ISC (a.u)
% of γH2Av^high ISCs
Control
RnrL KD1
RnrL KD2
Stem cell driver (Delta^ts) > FUCCI, 2 days
DAPI RFP GFP γH2Av
FUCCI
γH2Av
Control
RnrL KD2
E
E'
E''
F
F'
F''
FUCCI:
G1
S
G2
G
2 days
4 days
Proportion of ISC in each cell cycle phases (%)
Cell Cycle Phases:
G2
S
G1
H
G1
S
G2
γH2Av intensity in ISC (a.u)
Stem cell driver (Delta^ts) > RFP, 2 days
DAPI RFP
RpA70-GFP γH2Av
RFP
γH2Av
RpA70-GFP
Control
HU
I
I'
I''
I'''
J
J'
J''
J'''
K
γH2Av intensity in ISC (a.u)
RpA70-GFP Max Intensity
Control
HU
L
γH2Av^high
RpA70-GFP^high
Proportion of ISCs (%)
M
pH3+cells per gut
2 days
4 days

fig. S1. *RnrL* inhibition causes replication stress in midgut stem cells.
A-A''. *Su(H)GBE-LacZ* midguts stained for RnrL, ßGal, Armadillo (membrane), and Prospero (nuclear). ßGal is expressed in EBs (diploid, small nuclei) and persists in newly produced young ECs (yECs, polyploid, big nuclei). ISC are Arm+ ßGal-, EEs are Pros+, EB are Arm+ ßGal+, ECs are characterized by big nuclei. Scale bar: 25µm. **B.** Percentage of midgut cells with high or low levels of RnrL expression as seen by immunostaining in G-G''. yEC are newly produced ECs in which ßGal persists. **C.** γH2Av mean intensity in stem cell nuclei (Dl^{ts}>GFP+) without or with *RnrL* RNAi for 4 days, two different RNAi lines were tested, normalized to the mean value in the Control. Welch's t-test. **D.** Proportion of ISC (GFP+) with high levels of γH2Av (>2 of mean γH2Av intensity in C). Fisher's test. **E-F''.** $Delta^{ts}$>FUCCI midguts with (E) or without (F) *RnrL* RNAi for 2 days. Cells in G1 are marked by nuclear GFP, cells in S phase by cytoplasmic RFP and cells in G2 by both markers. **G.** Proportion of stem cells in each cell cycle phase from $Delta^{ts}$>FUCCI with or without *RnrL* RNAi after 2 or 4 days of *RnrL* knock down, two different RNAi lines were used. Chi-squared test. **H.** γH2Av mean intensity in each cell cycle phase after 2 days of *RnrL* RNAi or control in $Delta^{ts}$>FUCCI. Normalized to the mean of the Control. **I-J'''.** $Delta^{ts}$>RFP, RpA70-GFP female midguts fed with Control food (I-I'''), or HU-containing food (J-J''') for 2 days and stained for DAPI, RFP, γH2Av, and GFP. Scale bar: 20µm. **K.** γH2Av mean intensity and RpA70-GFP max intensity in each ISC (RFP+) nuclei in Control or HU condition. Normalized to the mean value in the Control. Welch's t-test. **L.** Proportion of ISC (RFP+) with high levels of γH2Av (>2 of mean γH2Av intensity in I) or RpA70-GFP (>3 of max RpA70-GFP intensity in I). Fisher's test. **M.** PH3+ cells per midgut in female flies fed with Control or HU containing food for 2 or 4 days. Welch's t-test. *: $p < 0.05$; **: $p < 0.01$; ***: $p<0.001$; ****: $p<0.0001$. N = guts, n = cells. Red crosses = mean.

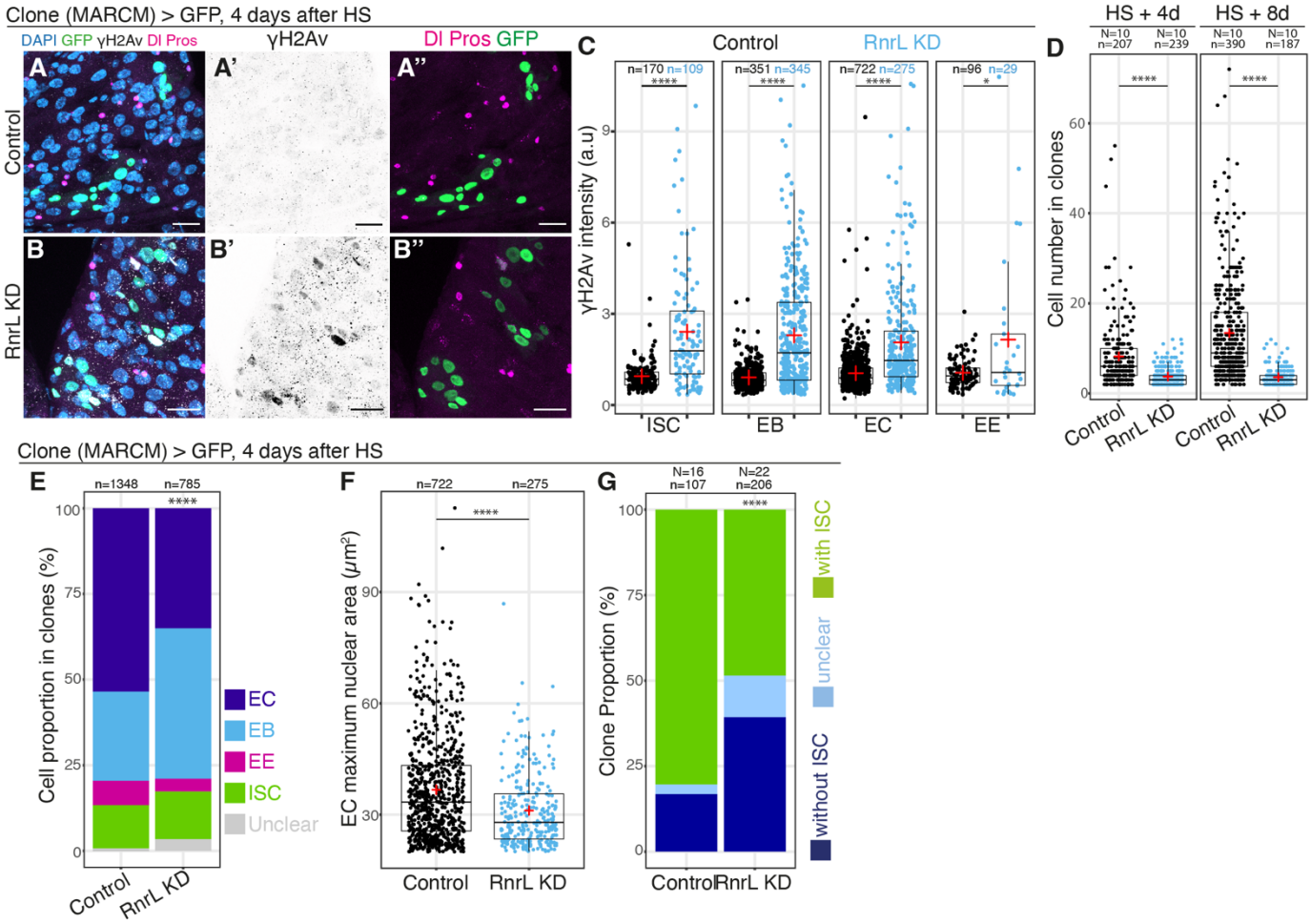

fig. S2. Clonal depletion of RnrL affects stem cells and progeny.
A-B''. Clones induced with the mosaic analysis of repressible cell marker system (MARCM>GFP) 4 days after heat-shock (induction) with or without *RnrL* RNAi, stained for DAPI, GFP, γH2Av, Delta (Dl, membrane vesicles) and Pros (nuclear). Stem cells are marked with Dl and EEs with Pros. γH2Av indicates DNA damage. Scale bar: 20µm. **C.** γH2Av mean intensity in each cell types in the clones, normalized to Control mean of all cells. Welch's t-test. Clonal depletion of *RnrL* also resulted in high levels of DNA damage, which was especially prominent in ISCs and EBs, but also occurred in ECs and EEs. **D.** Cell number per clone (clone size) 4 days or 8 days after heat-shock in Control or *RnrL* RNAi conditions. Welch's t-test. The size of the clone was reduced in *RnrL* RNAi conditions. **E.** Cell composition of MARCM>GFP clones with or without *RnrL* RNAi. Chi-square test. The cells for which the Dl staining was not clearly positive (ISC) or negative (EB) were classified as "Unclear". The proportion of differentiated cells (EEs and ECs) was reduced. **F.** EC nuclear size in MARCM>GFP clones with or without *RnrL* RNAi. Welch's t-test. The size of EC nuclei was reduced consistent with nucleotide depletion affecting EC polyploidization which requires replication. **G.** Proportion of clones with or without stem cells, 4 days after clone induction in Control and *RnrL* RNAi conditions. Stem cells were detected with Dl staining. The clones with cells for which the Dl staining was not clearly positive (ISC) or negative (not ISC) were classified as "unclear". Fisher's test. The proportion of clones without stem cell is increased upon RnrL KD, consistent with ISC loss.
*: $p < 0.05$; **: $p < 0.01$; ***: $p < 0.001$; ****: $p < 0.0001$. N = guts, n = cells. Red crosses = mean

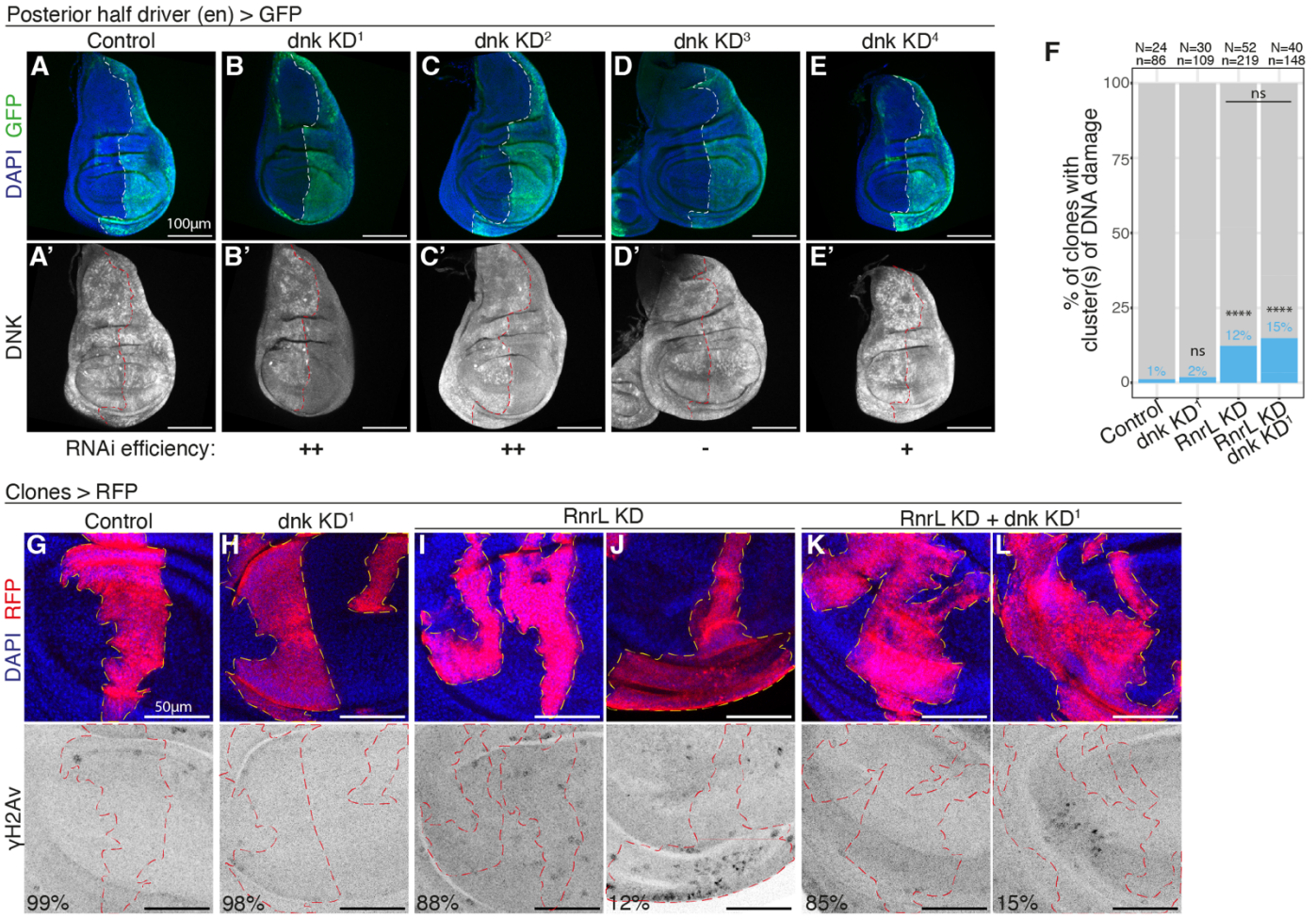

fig. S3. Inhibition of de novo dNTP synthesis is not rescued by salvage pathway activity.
A-E'. Test of *dnk* RNAi efficiency. *en>GFP* Control discs (w^{1118}, A-A'), and discs expressing four different *dnk* RNAi (B-E') stained for DAPI, GFP and DNK. The *dnk* KD 1 (B-B') and 2 (C-C') showed loss of DNK staining indicating an efficient knockdown of *dnk*. The *dnk* RNAi line 3 (D-D') does not working while the 4th RNAi (E-E') has partial efficiency as DNK staining was reduced. The *dnk* KD^1 was used for the rest of the paper. Scale bar: 100µm. **F.** Percentage of clones displaying clusters of cells with DNA damage (γH2Av). N = wing discs, n= clones. Fisher's test. **G-L.** hs-FlipOut>RFP clones in the late third instar larval wing disc, 4 days after induction in first instar larvae and stained for DAPI, RFP and γH2Av, with Control clones (G-G'), *dnk* RNAi (H-H'), *RnrL* RNAi (I-J'), and *dnk* & *RnrL* RNAi (K-L'). While most clones with *RnrL* RNAi or *dnk* & *RnrL* RNAi had no DNA damage (I-I', K-K'), a minority of clones displayed clusters of cells with higher level of γH2Av (J-J', L-L'). Scale bar: 50µm. *: $p < 0.05$; **: $p < 0.01$; ***: $p < 0.001$; ****: $p < 0.0001$.

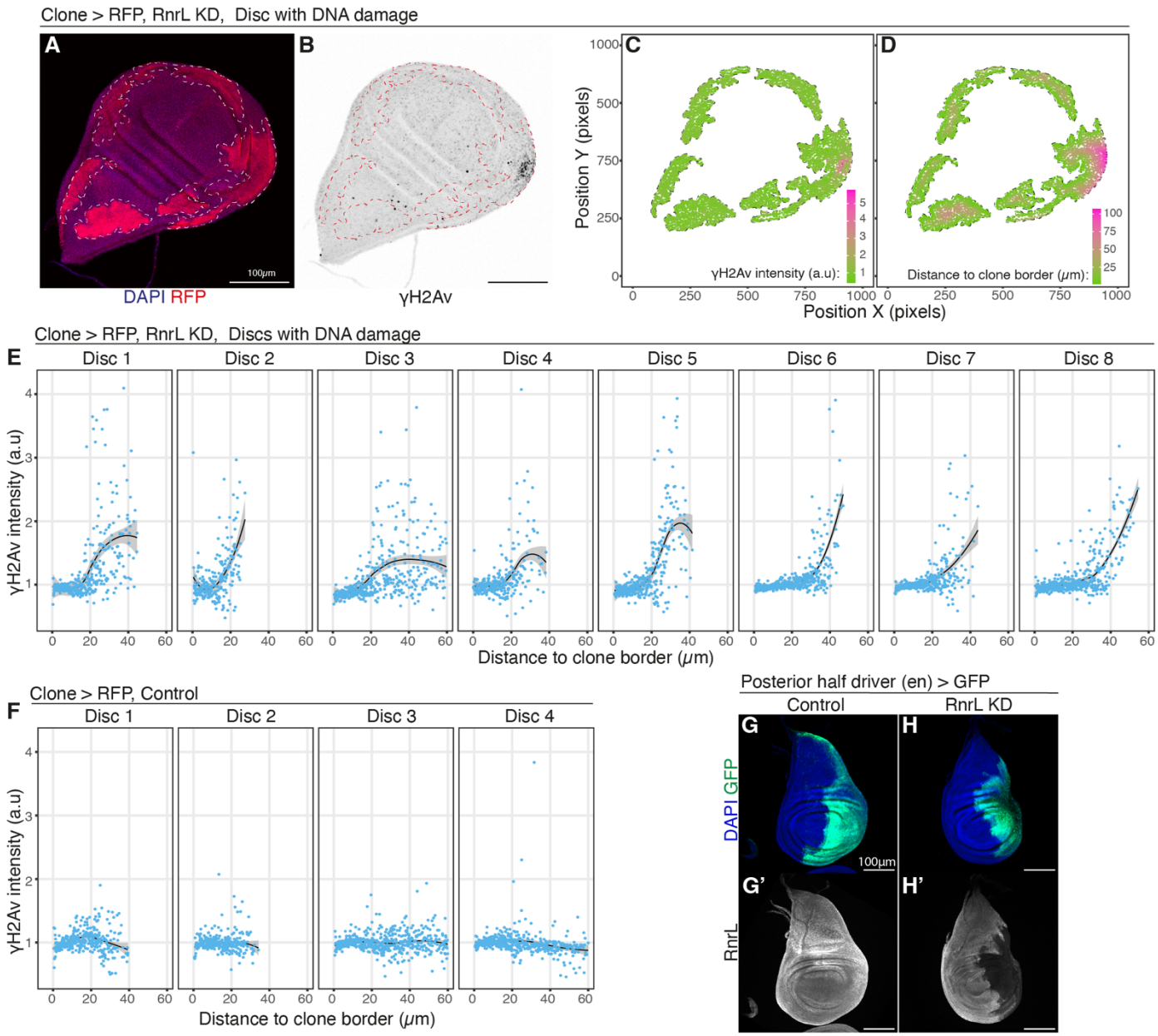

fig. S4. DNA damage localization suggests a non-cell autonomous rescue of nucleotides.
A-B. hs-FlipOut>RFP clones expressing *RnrL* RNAi in the wing disc, 4 days after induction in larvae and stained for DAPI, RFP (A) and γH2Av (B). Scale bar: 100µm. **C-D.** In silico mapping of the RFP+ wing disc clones, for cells within the clones, measure of the mean γH2Av intensity (C), and closest distance to the non-clonal wild-type tissue outside of the RFP+ clone (D). **E-F.** Mean γH2Av intensity per cells in the clones relative to the distance to the wild-type surrounding tissue (clone border), in 8 different discs expressing *RnrL* RNAi in clones that displayed DNA damage (E), and 4 Control wild-type wing discs without DNA damage (F). For each wing disc, the black line is the LOESS curve of local regression (y ~ x) and the gray area represents a 0.95 confidence interval. The value is normalized to the mean γH2Av intensity in wild-type non clonal tissue (outside of the clones) for each wing discs. DNA damage was found more than 20-35µm from the clone border. **G-H.** *en>GFP* Control discs (w^{1118}, G-G'), and discs expressing four *RnrL* RNAi (H-H'') stained for DAPI, GFP and RnrL. RnrL is lost throughout the engrailed (GFP+) domain in the *RnrL* KD condition.

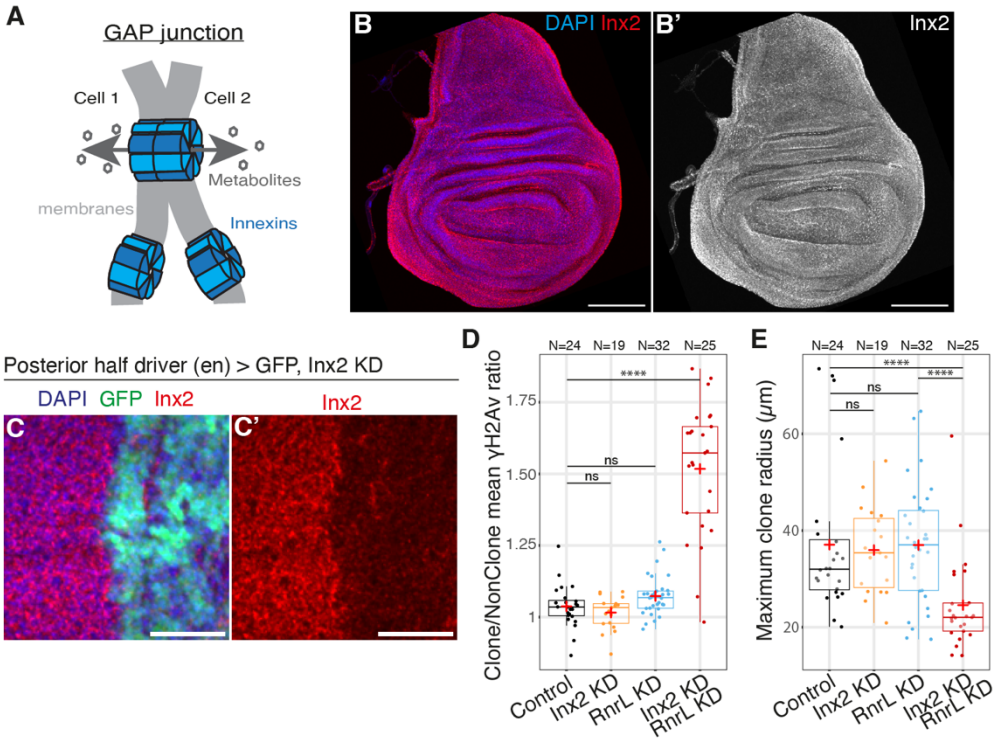

fig. S5. A role for gap junctions in nucleotide sharing between wing disc cells.
A. Representation of a *Drosophila* gap junction formed by innexin proteins. **B-B'.** *Drosophila* late third instar larval wing disc stained for DAPI and Inx2. Scale bar: 100µm. **C-C'.** *en>GFP* wing discs expressing *Inx2* RNAi in the engrailed GFP+ domain, stained for Inx2. Close up of the pouch area. Scale bar: 30µm. **D.** Mean γH2Av intensity ratio between clones (RFP+) and non-clonal wild type tissue for each wing disc analyzed, in hs-FlipOut RFP+ Control, *Inx2* KD, *RnrL* KD or *Inx2* & *RnrL* KD clones. Welch's t-test. **E.** Maximum distance (µm) of clone cells to the clone border (WT tissue) in hs-FlipOut RFP+ clones of the wing disc, as a proxy for clone radius/size. Welch's t-test.
*: $p < 0.05$; **: $p < 0.01$; ***: $p < 0.001$; ****: $p < 0.0001$. N = discs. Red cross = mean.

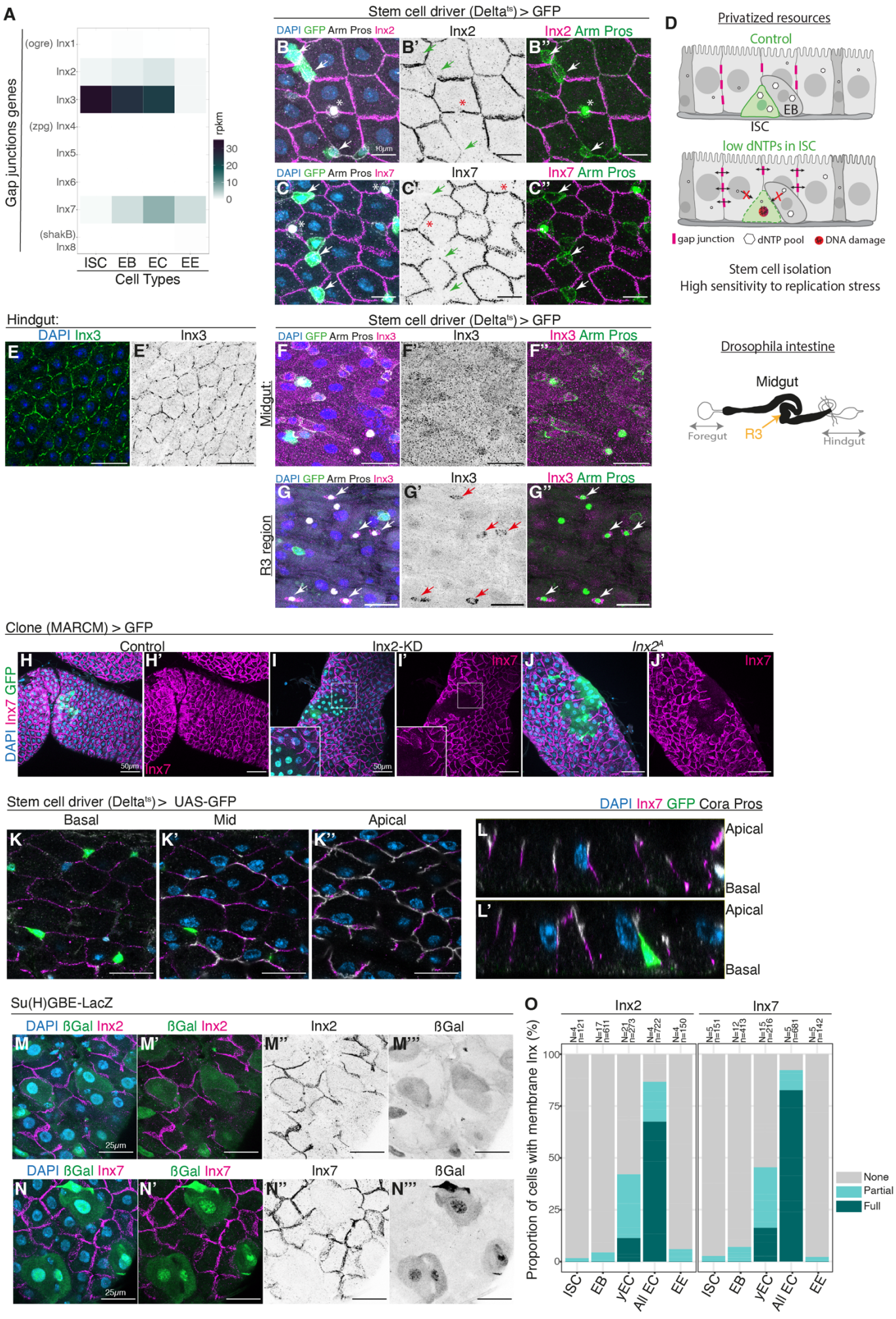
A
Gap junctions genes
(ogre) Inx1
Inx2
Inx3
(zpg) Inx4
Inx5
Inx6
Inx7
(shakB) Inx8
rpkm
30
20
10
0
ISC EB EC EE
Cell Types
Stem cell driver (Delta^{ts}) > GFP
DAPI GFP Arm Pros Inx2
Inx2
Inx2 Arm Pros
DAPI GFP Arm Pros Inx7
Inx7
Inx7 Arm Pros
10μm
D
Privatized resources
Control
EB
ISC
low dNTPs in ISC
gap junction
dNTP pool
DNA damage
Stem cell isolation
High sensitivity to replication stress
Hindgut:
DAPI Inx3
Inx3
Stem cell driver (Delta^{ts}) > GFP
DAPI GFP Arm Pros Inx3
Inx3
Inx3 Arm Pros
Midgut:
R3 region
Drosophila intestine
Midgut
Foregut
R3
Hindgut
Clone (MARCM) > GFP
Control
Inx2-KD
Inx2^{4}
DAPI Inx7 GFP
Inx7
50μm
Stem cell driver (Delta^{ts}) > UAS-GFP
DAPI Inx7 GFP Cora Pros
Basal
Mid
Apical
Su(H)GBE-LacZ
DAPI ßGal Inx2
ßGal Inx2
Inx2
ßGal
DAPI ßGal Inx7
ßGal Inx7
Inx7
ßGal
25μm
O
Inx2
Inx7
Proportion of cells with membrane Inx (%)
100
75
50
25
0
ISC
EB
yEC
All EC
EE
None
Partial
Full

fig. S6. *Drosophila* intestinal stem cells lack gap junctions.
A. Expression levels of the 8 Innexin genes in the intestinal cell types (data from Dutta et al. 2015). *Inx2*, *Inx3*, and *Inx7* genes are expressed in the midgut **B-C''.** *Delta^{ts}>GFP* female midguts stained for DAPI, GFP, Armadillo (membrane), Prospero (nuclear) and Inx2 (A-A'') or Inx7 (B-B''). *Delta^{ts}* drives GFP expression in the intestinal stem cells (white/green arrows), Prospero marks enteroendocrine cells (white/red asterisks), and the ß-catenin Armadillo is enriched at the membrane of diploid cells (Intestinal stem cells and Enteroblasts). Inx2 and Inx7 were only found at the membrane of large polyploid enterocytes. Membrane location of Inx2 and Inx7 was undetectable in ISCs (arrows), similarly, Inx2 and Inx7 were absent at the membranes of the diploid EBs and Prospero-expressing enteroendocrine cells (asterisks). Scale bar: 10µm. **D.** Model of midgut epithelium, ISC are isolated from the rest of the midgut epithelium. As they lack gap junctions, they do not share resources with neighboring cells. ISC (Intestinal Stem Cell), EB (Enteroblast). **E-E'.** Membrane localization of Inx3 staining in the hindgut, consistent with formation of gap junction in this tissue. Scale bar: 20µm. **F-G'''.** *Delta^{ts}>GFP* female midguts stained for DAPI, GFP, Inx3, Armadillo (membrane) and Prospero (nuclear). *Delta^{ts}* drives GFP expression in the ISCs, Prospero marks Enteroendocrine cells, and the ß-catenin Armadillo is enriched at the membrane of diploid cells (Intestinal stem cells and Enteroblasts). Inx3 appeared to form intracellular puncta in all the cells and was not enriched at any cell membranes (F-F''), with the exception of a small population of enteroendocrine (EE) cells in the middle midgut (R3 region) that had high levels of Inx3 throughout the cell (arrows, G-G'). Thus, Inx3 likely does not form gap junctions in the midgut. Scale bar: 20µm. **H-J'.** MARCM>GFP clones in midguts stained for Inx7. Control clone (H-H'), *Inx2* RNAi clone (I-I'), *Inx2^{A}* clone (J-J'). The loss of *Inx2* function in clones resulted in absence of Inx7 immunoreactivity in clones and of Inx7 membrane localization in adjacent wildtype cells. Thus, Inx2 and Inx7 form gap junctions between neighboring ECs and suggests that Inx2 is required for Inx7 accumulation in the cell. Scale bar: 50µm. **K-L'.** *Delta^{ts}>GFP* midguts stained for Inx7 for gap junctions and Coracle for septate junctions. Different views of the epithelium, basal (K), intermediate (K') and apical (K''), as well as orthogonal reconstitution from the Z-stack (L-L'). Inx2 and Inx7 proteins localized at the basal membranes below septate junctions in ECs. Scale bar: 20µm. **M-N'''.** *Su(H)GBE-LacZ* midguts stained for Inx2 (M-M') or Inx7 (N-N'). ßGal is expressed in EBs (diploid, small nuclei) and persists in newly made ECs (polyploid, big nuclei). Inx2 and Inx7 were found to be present only between the membranes of mature EC cells and absent from young ECs. Scale bar: 25µm. **O.** Quantification of the proportion of cells with partial or full membrane staining of Inx2 and Inx7 in ISC (Arm+, ßGal-, small nucleus), EB (Arm+, ßGal+, small nucleus), young Enterocytes (ßGal+, big nucleus), all Enterocytes (big nucleus) and EEs (Pros+). N = guts, n = cells.

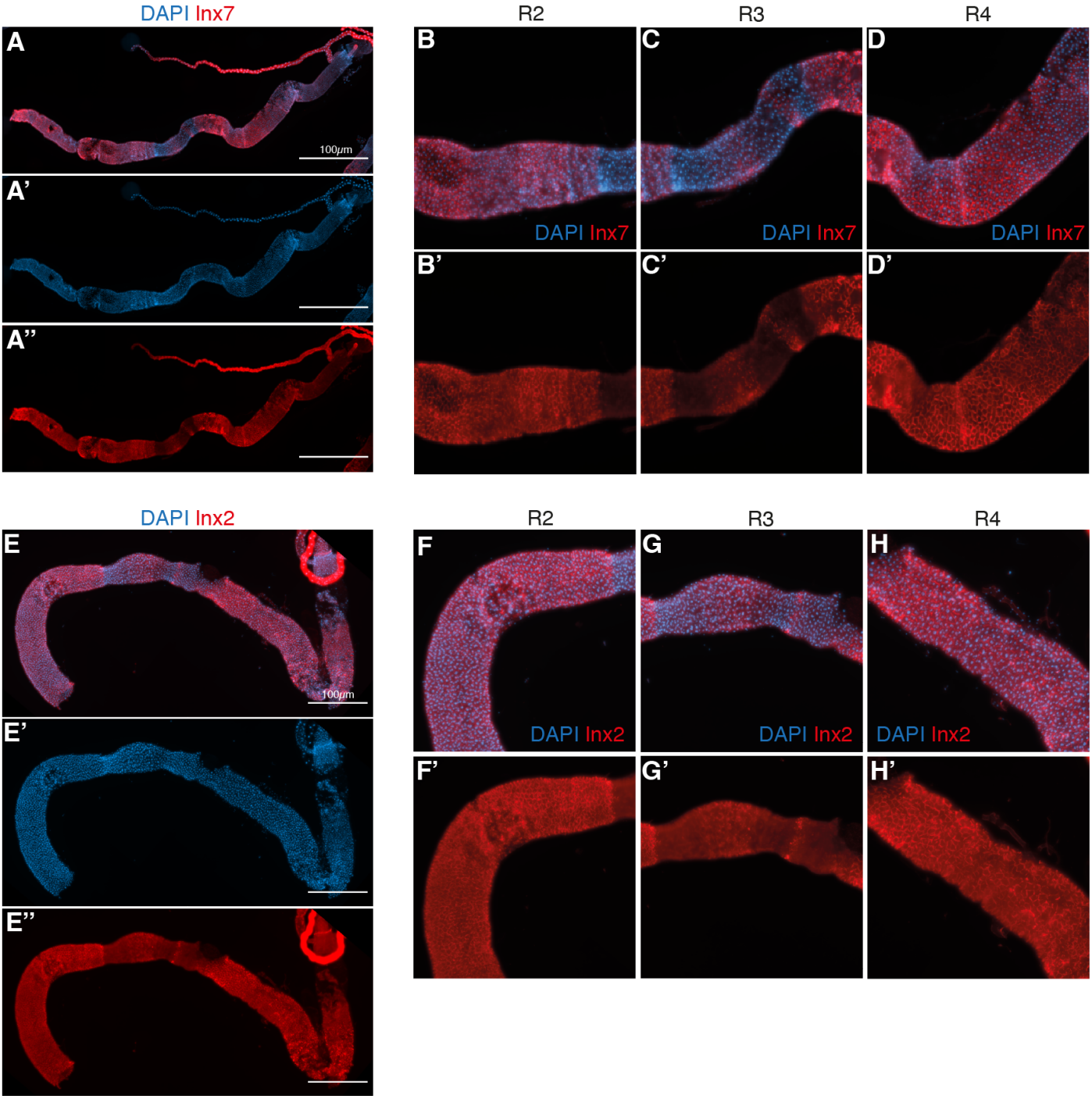

fig. S7. Regional differences in gap junction expression in the midgut. A-D'. Inx7 staining in whole guts (A-A'') and in close ups of anterior region (R2, B-B'), mid/copper cell region (R3, C-C') and posterior (R4, D-D'). **E-H'.** Inx2 staining in whole guts (E-E'') and in close ups of anterior region (R2, F-F'), mid/copper cell region (R3, G-G') and posterior (R4, H-H'). Scale bars: 100µm. Inx2 and Inx7 were found to be highly expressed in R2 and R4 regions, expressed in R3, and absent in the R5 region of the midgut. Interestingly, different regions are separated by clear stripes lacking gap junction expression, likely separating different functional domains. A thin band of expression is found between R3 and R4 regions between two domains lacking expression.

Twin-Spot clones in ubiRFP discs

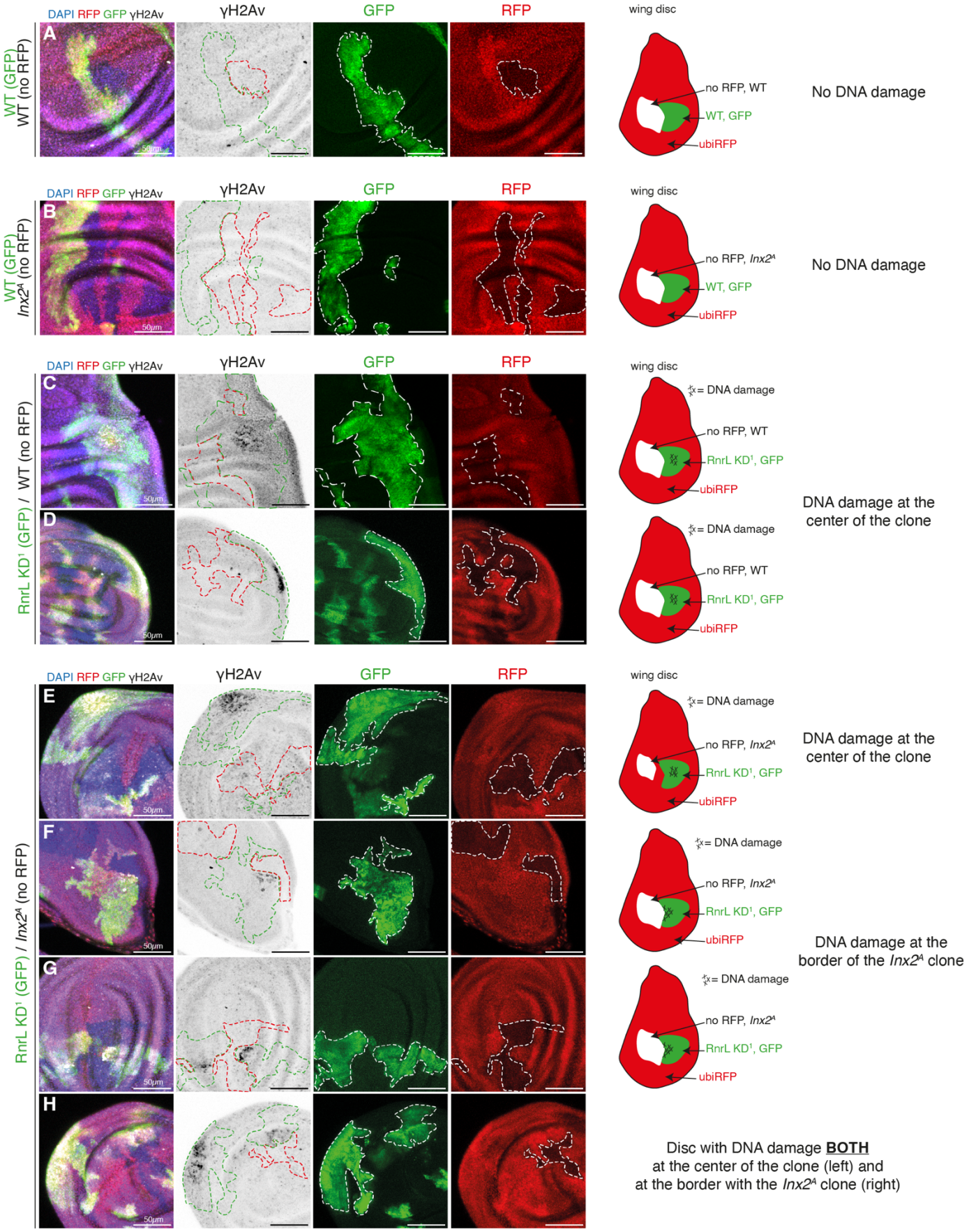

fig. S8. Twin spot-clones in the wing disc.
Examples of twin-spot clones in the wing disc 4 days after induction in larvae and stained for DAPI, GFP, RFP and γH2Av. As indicated in the schematic, while the tissue expresses RFP ubiquitously, upon clone induction, one clone loses the RFP expression and remains wild-type (WT; A, C-D) or becomes *Inx2*^{A} homozygous mutant (B, E-H), and the twin-clone obtains Gal4/UAS driven expression of GFP with (C-H) or without (A, B) *RnrL* RNAi. Resulting in the corresponding genotype for each induced clones: WT/WT (A), WT/*Inx2*^{A} (B), *RnrL* RNAi/WT (C, D) and *RnrL* RNAi/*Inx2*^{A} *(E-H)*. The controls A-B had no DNA damage.

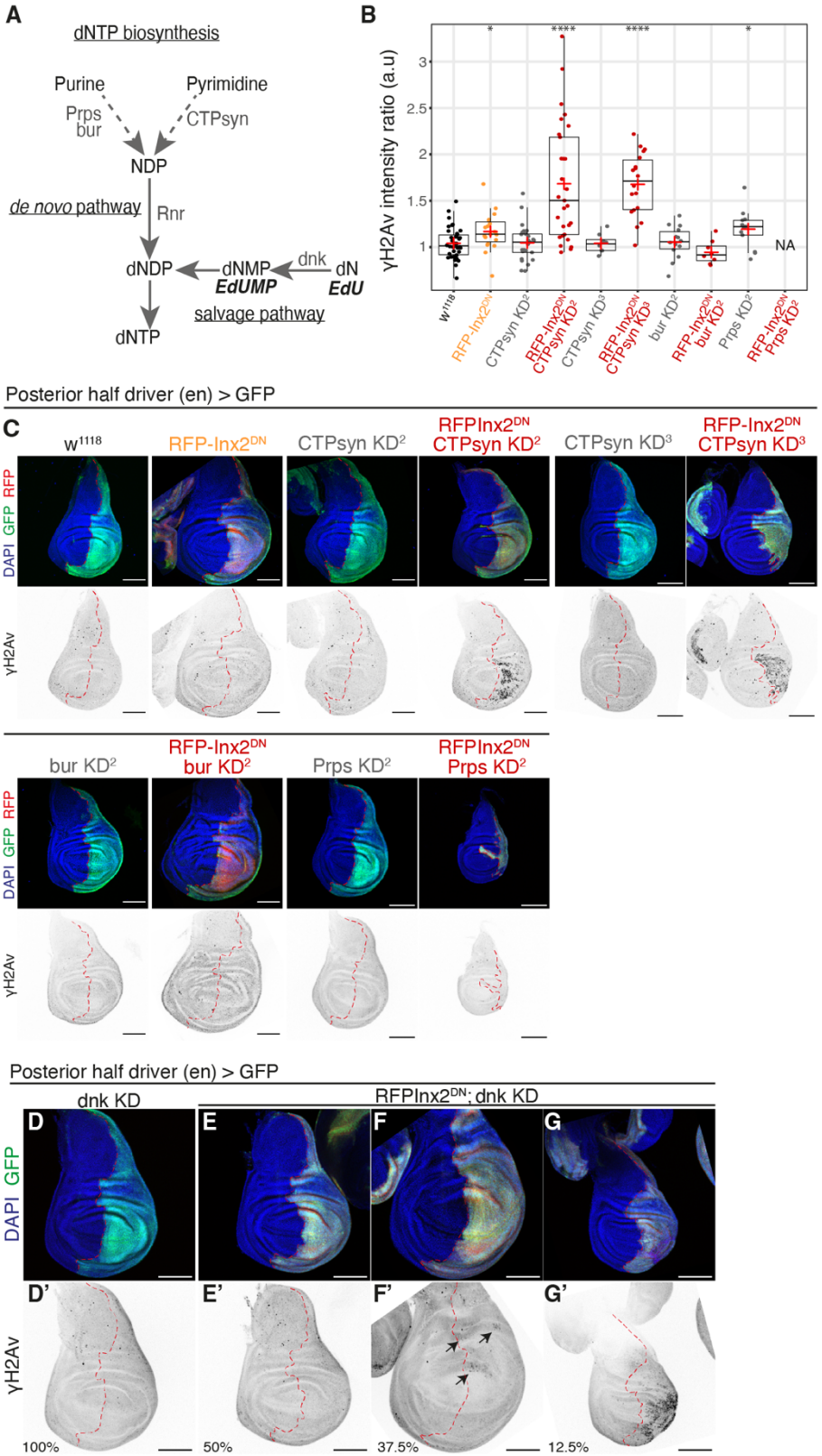

fig. S9. Nucleotide sharing through gap junctions in the wing disc epithelium.

A. Simplified representation of the dNTP biosynthesis pathways and enzymes. **B.** γH2Av mean intensity in the pouch region of the engrailed domain (posterior, GFP+) relative to the mean intensity in the pouch region of the non-engrailed domain (anterior, GFP-). Welch's t-test. **C.** *en>GFP* control discs (w^{1118}), disc expressing a dominant negative form of Inx2 ($RFPInx2^{DN}$) in combination with *CTP synthetase* RNAi, *bur* RNAi or *Prps* RNAi. The discs were dissected at late third instar larval stage and stained for γH2Av. Scale bar: 100µm. **D-G'.** *en>GFP* disc expressing *dnk* RNAi alone (D-D') or in combination with a dominant negative form of Inx2 ($RFPInx2^{DN}$, E-G'). The discs were dissected at late third instar larval stage and stained for γH2Av. While discs with *dnk* RNAi alone did not have DNA damage (N=15, E-E'), 50% of the discs with *dnk* RNAi and $RFPInx2^{DN}$ displayed an increase in DNA damage, in small clusters of cells (37.5%, N=6/16, arrows in F-F'), or in most of the engrailed domain (12.5%, N=2/16, G-G'). Scale bar: 100µm.
*: $p < 0.05$; **: $p < 0.01$; ***: $p < 0.001$; ****: $p < 0.0001$. N = discs. Red cross = mean

Table S1. List of fly stocks used in the paper.

Name	Genotype	Source-Reference
RnrL KD-1	y[1] sc[*] v[1];; P{y[+t7.7] v[+t1.8]=TRiP.HMC02351}attP2	BL51418
RnrL KD-2	y[1] sc[*] v[1]; P{y[+t7.7] v[+t1.8]=TRiP.HMS02737}attP40	BL44022
Inx2 KD	;; UAS-Inx2 RNAi TRIP JF02446	P. Spéder (formerly BL28915)
RFP-Inx2DN	; pTRW-inx2 UAS-RFP-inx2 (RI1)	A. Brand/P. Spéder
CTPsyn KD-1	y[1] v[1]; P{y[+t7.7] v[+t1.8]=TRiP.HMJ02094}attP40	BL53378
CTPsyn KD-2	y[1] v[1];; P{y[+t7.7] v[+t1.8]=TRiP.HM04062}attP2	BL31752
CTPsyn KD-3	y[1] v[1];; P{y[+t7.7] v[+t1.8]=TRiP.JF02214}attP2	BL31924
Prps KD-1	y[1] sc[*] v[1] sev[21]; P{y[+t7.7] v[+t1.8]=TRiP.HMC05080}attP40	BL60086
Prps KD-2	y[1] sc[*] v[1] sev[21];; P{y[+t7.7] v[+t1.8]=TRiP.GL00463}attP2/TM3, Sb[1]	BL35619
dnk KD-1	w[1118];; P{GD15092}v39137	v39137
dnk KD-2	; P{KK100376}VIE-260B	v103385
dnk KD-3	y[1] sc[*] v[1] sev[21]; P{y[+t7.7] v[+t1.8]=TRiP.HMC06148}attP40	BL65886
dnk KD-4	y[1] sc[*] v[1] sev[21];; P{y[+t7.7] v[+t1.8]=TRiP.GL00100}attP2	BL35219
bur KD-1	y[1] v[1]; P{y[+t7.7] v[+t1.8]=TRiP.HMJ22744}attP40 bur RNAi	BL60432
bur KD-2	y[1] v[1];; P{y[+t7.7] v[+t1.8]=TRiP.JF01503}attP2	BL31055
w1118	w[1118]	M. McVey
EnGal4 GFP	w[*] ; P[En-Gal4], P[UAS-GFP]/CyO, w+, Tb	Y. Bellaiche, P. Leopold
Inx2A FRT19A	y[1] w[*] Inx2[A] P{ry[+t7.2]=neoFRT}19A/FM7c, P{w[+mC]=GAL4-Kr.C}DC1, P{w[+mC]=UAS-GFP.S65T}DC5, sn[+]	BL54481
DlGal4	;; P[Delta-Gal4]/TM6 Tb	S. Hou
UAS-GFP	w[*]; P{w[+mC]=UAS-2xEGFP}AH2	BL6874
UAS-nlsRFP	w[1118]; P{w[+mC]=UAS-RFP.W}2	BL30556
Dlts GFP	w[*] ; P{w[+mC]=UAS-2xEGFP}AH2/(CyO) ; P[Delta-Gal4], tub-gal80ts/TM6B, Tb, Hu	This study
Dlts RFP	w[*] ; P{w[+mC]=UAS-RFP.W}2/ (CyO) ; P[Delta-Gal4], tub-gal80ts/TM6B, Tb, Hu	This study
Dlts FUCCI	w[*] ; UASt-GFP-E2F1$_{1-230}$#32 UASt-mRFP1-CycB$_{1-266}$#13 ; P[Delta-Gal4], tub-gal80ts/TM6B, Tb, Hu	This study
FUCCI	; UASt-GFP-E2F1 , UASt-RFP-CycA-nls ; MKRS/TM6	B. Edgar
RpA70-GFP	;; RPA-70::EGFP	A. M. Vales
TwinSpot driver	P{w[+mC]=Ubi-mRFP.nls}1, w[*], P{ry[+t7.2]=hsFLP}12 P{ry[+t7.2]=neoFRT}19A ; P{w[+mC]=Act5C-GAL4}25FO1, P{w[+mC]=UAS-GFP.U}2/CyO	This study (from BL42726, BL31406)
TwinSpot WT/WT	P{w[+mC]=tubP-GAL80}LL1 y[1] w[*] P{ry[+t7.2]=neoFRT}19A	This study (from BL42726)
TwinSpot WT/Inx2A	P{w[+mC]=tubP-GAL80}LL1 y[1] w[*] Inx2[A] P{ry[+t7.2]=neoFRT}19A	This study (from BL42726, BL54481)
TwinSpot RnrL KD/WT	P{w[+mC]=tubP-GAL80}LL1 y[1] w[*] P{ry[+t7.2]=neoFRT}19A ;; P{y[+t7.7] v[+t1.8]=TRiP.HMC02351}attP2	This study (from BL42726, BL51418)
TwinSpot RnrL KD/Inx2A	P{w[+mC]=tubP-GAL80}LL1 y[1] w[*] Inx2[A] P{ry[+t7.2]=neoFRT}19A/FM7-GFP ;; P{y[+t7.7] v[+t1.8]=TRiP.HMC02351}attP2	This study (from BL42726, BL54481, BL51418)

Su(H)GBE-LacZ	;Su(H)GBE-LacZ	S. Bray
MARCM40A	yw [hs-Flp]1.22 P[Tub-FRT-Gal4] P[UAS-nlsGFP]/(FM6) ; P{tubP-GAL80}LL10 P{neoFRT}40A/(CyO)	Bardin et al. 2010 (from BL5192)
FRT40A	; {neoFRT}40A [mw]/ (CyO)	Bardin et al. 2010
hs-FlipOut RFP	hs-flp ;; Tub-FRT-Gal80-FRT-Gal4, UAS-mRFP/TM6b, Tb, Hu	Y. Bellaiche, gift of E. Martin-Blanco
MARCM19A	p{ry[+] neoFRT}19A, P{w[+] tubP-GAL80}L1, P{ry[+] hsFLP}1, w ; CyO/P{w[+] UAS-CD8:GFP}LL5 ; TM6, Tb, Hu / P{w[+] tubP-GAL4}LL7	A. Gould

Table S2. List of genotypes per figures.

Figure	Panel	Condition	Genotype
1	B	Control	; P{w[+mC]=UAS-RFP.W}2/+ ; P[Delta-Gal4], tub-gal80ts/RPA-70::EGFP
	C	RnrL KD-2	; P{w[+mC]=UAS-RFP.W}2/P{y[+t7.7] v[+t1.8]=TRiP.HMS02737}attP40; P[Delta-Gal4], tub-gal80ts/RPA-70::EGFP
	D, E	Control	; P{w[+mC]=UAS-RFP.W}2/+ ; P[Delta-Gal4], tub-gal80ts/RPA-70::EGFP
		RnrL KD-2	; P{w[+mC]=UAS-RFP.W}2/P{y[+t7.7] v[+t1.8]=TRiP.HMS02737}attP40; P[Delta-Gal4], tub-gal80ts/RPA-70::EGFP
	F	Control	w[*] ; P{w[+mC]=UAS-2xEGFP}AH2/+ ; P[Delta-Gal4], tub-gal80ts/+
	G	RnrL KD-2	w[*] ; P{w[+mC]=UAS-2xEGFP}AH2/P{y[+t7.7] v[+t1.8]=TRiP.HMS02737}attP40 ; P[Delta-Gal4], tub-gal80ts/+
	H	Control	w[*] ; P{w[+mC]=UAS-2xEGFP}AH2/+ ; P[Delta-Gal4], tub-gal80ts/+
		RnrL KD-2	w[*] ; P{w[+mC]=UAS-2xEGFP}AH2/P{y[+t7.7] v[+t1.8]=TRiP.HMS02737}attP40 ; P[Delta-Gal4], tub-gal80ts/+
2	B	Control	hs-flp ;; Tub-FRT-Gal80-FRT-Gal4, UAS-mRFP/+
	C, D	RnrL KD-2	hs-flp ; P{y[+t7.7] v[+t1.8]=TRiP.HMS02737}attP40/+; Tub-FRT-Gal80-FRT-Gal4, UAS-mRFP/+
	E, F	Control	hs-flp ;; Tub-FRT-Gal80-FRT-Gal4, UAS-mRFP/+
		RnrL KD-1	hs-flp ; P{y[+t7.7] v[+t1.8]=TRiP.HMS02737}attP40/+; Tub-FRT-Gal80-FRT-Gal4, UAS-mRFP/+
	G	Control	hs-flp ;; Tub-FRT-Gal80-FRT-Gal4, UAS-mRFP/+
		RnrL KD-2	hs-flp ; P{y[+t7.7] v[+t1.8]=TRiP.HMS02737}attP40/+; Tub-FRT-Gal80-FRT-Gal4, UAS-mRFP/+
	H	Control	w[*] ; P[En-Gal4], P[UAS-GFP]/+
	I	RnrL KD-1	; P[En-Gal4], P[UAS-GFP]/+ ; P{y[+t7.7] v[+t1.8]=TRiP.HMC02351}attP2/+
	J	RnrL KD-2	; P[En-Gal4], P[UAS-GFP]/P{y[+t7.7] v[+t1.8]=TRiP.HMS02737}attP40
	K	Control	w[*] ; P[En-Gal4], P[UAS-GFP]/+
		RnrL KD-1	; P[En-Gal4], P[UAS-GFP]/+ ; P{y[+t7.7] v[+t1.8]=TRiP.HMC02351}attP2/+
		RnrL KD-2	; P[En-Gal4], P[UAS-GFP]/P{y[+t7.7] v[+t1.8]=TRiP.HMS02737}attP40
3	A	Control	hs-flp ;; Tub-FRT-Gal80-FRT-Gal4, UAS-mRFP/+
	B, C	RnrL KD-2	hs-flp ; P{y[+t7.7] v[+t1.8]=TRiP.HMS02737}attP40/+; Tub-FRT-Gal80-FRT-Gal4, UAS-mRFP/+
	D	Inx2 KD	hs-flp ;; Tub-FRT-Gal80-FRT-Gal4, UAS-mRFP/UAS-Inx2 RNAi TRIP JF02446
	E	RnrL KD-2 ; Inx2 KD	hs-flp ; P{y[+t7.7] v[+t1.8]=TRiP.HMS02737}attP40/+; Tub-FRT-Gal80-FRT-Gal4, UAS-mRFP/UAS-Inx2 RNAi TRIP JF02446
	F	Control	hs-flp ;; Tub-FRT-Gal80-FRT-Gal4, UAS-mRFP/+
		RnrL KD-2	hs-flp ;; Tub-FRT-Gal80-FRT-Gal4, UAS-mRFP/UAS-Inx2 RNAi TRIP JF02446
		Inx2 KD	hs-flp ; P{y[+t7.7] v[+t1.8]=TRiP.HMS02737}attP40/+; Tub-FRT-Gal80-FRT-Gal4, UAS-mRFP/+
		RnrL KD-2 ; Inx2 KD	hs-flp ; P{y[+t7.7] v[+t1.8]=TRiP.HMS02737}attP40/+; Tub-FRT-Gal80-FRT-Gal4, UAS-mRFP/UAS-Inx2 RNAi TRIP JF02446
	G	RnrL KD-1/WT	P{w[+mC]=Ubi-mRFP.nls}1, w[*], P{ry[+t7.2]=hsFLP}12 P{ry[+t7.2]=neoFRT}19A/P{w[+mC]=tubP-GAL80}LL1 y[1] w[*] P{ry[+t7.2]=neoFRT}19A ; P{w[+mC]=Act5C-GAL4}25FO1, P{w[+mC]=UAS-GFP.U}2/+ ; P{y[+t7.7] v[+t1.8]=TRiP.HMC02351}attP2/+
	H	RnrL KD-1/Inx2A mutant	P{w[+mC]=Ubi-mRFP.nls}1, w[*], P{ry[+t7.2]=hsFLP}12 P{ry[+t7.2]=neoFRT}19A/P{w[+mC]=tubP-GAL80}LL1 y[1] w[*] Inx2[A] P{ry[+t7.2]=neoFRT}19A ; P{w[+mC]=Act5C-GAL4}25FO1, P{w[+mC]=UAS-GFP.U}2/P{y[+t7.7] v[+t1.8]=TRiP.HMC02351}attP2/+
	I	WT/WT	P{w[+mC]=Ubi-mRFP.nls}1, w[*], P{ry[+t7.2]=hsFLP}12 P{ry[+t7.2]=neoFRT}19A/P{w[+mC]=tubP-GAL80}LL1 y[1] w[*] P{ry[+t7.2]=neoFRT}19A ; P{w[+mC]=Act5C-GAL4}25FO1, P{w[+mC]=UAS-GFP.U}2/+
		WT/Inx2A mutant	P{w[+mC]=Ubi-mRFP.nls}1, w[*], P{ry[+t7.2]=hsFLP}12 P{ry[+t7.2]=neoFRT}19A/P{w[+mC]=tubP-GAL80}LL1 y[1] w[*] Inx2[A] P{ry[+t7.2]=neoFRT}19A ; P{w[+mC]=Act5C-GAL4}25FO1, P{w[+mC]=UAS-GFP.U}2/+
		RnrL KD-1/WT	P{w[+mC]=Ubi-mRFP.nls}1, w[*], P{ry[+t7.2]=hsFLP}12 P{ry[+t7.2]=neoFRT}19A/P{w[+mC]=tubP-GAL80}LL1 y[1] w[*] P{ry[+t7.2]=neoFRT}19A ; P{w[+mC]=Act5C-GAL4}25FO1, P{w[+mC]=UAS-GFP.U}2/+ ; P{y[+t7.7] v[+t1.8]=TRiP.HMC02351}attP2/+
		RnrL KD-1/Inx2A mutant	P{w[+mC]=Ubi-mRFP.nls}1, w[*], P{ry[+t7.2]=hsFLP}12 P{ry[+t7.2]=neoFRT}19A/P{w[+mC]=tubP-GAL80}LL1 y[1] w[*] Inx2[A] P{ry[+t7.2]=neoFRT}19A ; P{w[+mC]=Act5C-GAL4}25FO1, P{w[+mC]=UAS-GFP.U}2/P{y[+t7.7] v[+t1.8]=TRiP.HMC02351}attP2/+
4	A, B	Control	w[*] ; P[En-Gal4], P[UAS-GFP]/+
		Inx2 KD	w[*] ; P[En-Gal4], P[UAS-GFP]/+ ; UAS-Inx2 RNAi TRIP JF02446/+
		CTPsyn KD-1	w[*] ; P[En-Gal4], P[UAS-GFP]/ P{y[+t7.7] v[+t1.8]=TRiP.HMJ02094}attP40
		CTPsyn KD-1 ; Inx2 KD	w[*] ; P[En-Gal4], P[UAS-GFP]/ P{y[+t7.7] v[+t1.8]=TRiP.HMJ02094}attP40 ; UAS-Inx2 RNAi TRIP JF02446/+
		Prps KD-1	w[*] ; P[En-Gal4], P[UAS-GFP]/P{y[+t7.7] v[+t1.8]=TRiP.HMC05080}attP40

		Prps KD-1 ; Inx2 KD	w[*] ; P[En-Gal4], P[UAS-GFP]/P{y[+t7.7] v[+t1.8]=TRiP.HMC05080}attP40 ; UAS-Inx2 RNAi TRIP JF02446/+
		bur KD-1	w[*] ; P[En-Gal4], P[UAS-GFP]/P{y[+t7.7] v[+t1.8]=TRiP.HMJ22744}attP40
		bur KD-1 ; Inx2 KD	w[*] ; P[En-Gal4], P[UAS-GFP]/P{y[+t7.7] v[+t1.8]=TRiP.HMJ22744}attP40 ; UAS-Inx2 RNAi TRIP JF02446/+
	C	RFP-Inx2DN	w[*] ; P[En-Gal4], P[UAS-GFP]/pTRW-inx2 UAS-RFP-inx2 (RI1)
	D	dnk KD-1	w[*] ; P[En-Gal4], P[UAS-GFP]/+ ; P{GD15092}v39137/+
	E	RFP-Inx2DN ; dnk KD-1	w[*] ; P[En-Gal4], P[UAS-GFP]/pTRW-inx2 UAS-RFP-inx2 (RI1) ; P{GD15092}v39137/+
s1	A, B	NA	;Su(H)GBE-LacZ
	C, D	Control	w[*] ; P{w[+mC]=UAS-2xEGFP}AH2/+ ; P[Delta-Gal4], tub-gal80ts/+
		RnrL KD-1	w[*] ; P{w[+mC]=UAS-2xEGFP}AH2/+ ; P[Delta-Gal4], tub-gal80ts/P{y[+t7.7] v[+t1.8]=TRiP.HMC02351}attP2
		RnrL KD-2	w[*] ; P{w[+mC]=UAS-2xEGFP}AH2/P{y[+t7.7] v[+t1.8]=TRiP.HMS02737}attP40 ; P[Delta-Gal4], tub-gal80ts/+
	E	Control	w[*] ;UASt-GFP-E2F11-230#32 UASt-mRFP1-CycB1-266#13/+ ; P[Delta-Gal4], tub-gal80ts/+
	F	RnrL KD-2	w[*] ; UASt-GFP-E2F11-230#32 UASt-mRFP1-CycB1-266#13/P{y[+t7.7] v[+t1.8]=TRiP.HMS02737}attP40 ; P[Delta-Gal4], tub-gal80ts/+
	G, H	Control	w[*] ; UASt-GFP-E2F11-230#32 UASt-mRFP1-CycB1-266#13/+ ; P[Delta-Gal4], tub-gal80ts/+
		RnrL KD-1	w[*] ; UASt-GFP-E2F11-230#32 UASt-mRFP1-CycB1-266#13/+ ; P[Delta-Gal4], tub-gal80ts/P{y[+t7.7] v[+t1.8]=TRiP.HMC02351}attP2
		RnrL KD-2	w[*] ; UASt-GFP-E2F11-230#32 UASt-mRFP1-CycB1-266#13/P{y[+t7.7] v[+t1.8]=TRiP.HMS02737}attP40 ; P[Delta-Gal4], tub-gal80ts/+
	I-L	Control/HU	; P{w[+mC]=UAS-RFP.W}2/+ ; P[Delta-Gal4], tub-gal80ts/RPA-70::EGFP
	M	Control/HU	; P{w[+mC]=UAS-RFP.W}2/+ ; P[Delta-Gal4], tub-gal80ts/+
s2	A	Control	yw [hs-Flp]1.22 P[Tub-FRT-Gal4] P[UAS-nlsGFP]/(FM6) ; P{tubP-GAL80}LL10 P{neoFRT}40A/{neoFRT}40A [mw]
	B	RnrL KD-1	yw [hs-Flp]1.22 P[Tub-FRT-Gal4] P[UAS-nlsGFP]/(FM6) ; P{tubP-GAL80}LL10 P{neoFRT}40A/{neoFRT}40A [mw] ; P{y[+t7.7] v[+t1.8]=TRiP.HMC02351}attP2/+
	C-G	Control	yw [hs-Flp]1.22 P[Tub-FRT-Gal4] P[UAS-nlsGFP]/(FM6) ; P{tubP-GAL80}LL10 P{neoFRT}40A/{neoFRT}40A [mw]
		RnrL KD-1	yw [hs-Flp]1.22 P[Tub-FRT-Gal4] P[UAS-nlsGFP]/(FM6) ; P{tubP-GAL80}LL10 P{neoFRT}40A/{neoFRT}40A [mw] ; P{y[+t7.7] v[+t1.8]=TRiP.HMC02351}attP2/+
s3	A	Control	w[*] ; P[En-Gal4], P[UAS-GFP]/+
	B	dnk KD-1	w[*] ; P[En-Gal4], P[UAS-GFP]/+ ; P{GD15092}v39137/+
	C	dnk KD-2	w[*] ; P[En-Gal4], P[UAS-GFP]/P{KK100376}VIE-260B
	D	dnk KD-3	w[*] ; P[En-Gal4], P[UAS-GFP]/P{y[+t7.7] v[+t1.8]=TRiP.HMC06148}attP40
	E	dnk KD-4	w[*] ; P[En-Gal4], P[UAS-GFP]/+ ; P{y[+t7.7] v[+t1.8]=TRiP.GL00100}attP2/+
	F	*Control*	*hs-flp ;; Tub-FRT-Gal80-FRT-Gal4, UAS-mRFP/+*
		dnk KD-1	*hs-flp ;; Tub-FRT-Gal80-FRT-Gal4, UAS-mRFP/P{GD15092}v39137*
		RnrL KD-2	*hs-flp ; P{y[+t7.7] v[+t1.8]=TRiP.HMS02737}attP40/+; Tub-FRT-Gal80-FRT-Gal4, UAS-mRFP/+*
		RnrL KD-2 ; dnk KD-1	*hs-flp ; P{y[+t7.7] v[+t1.8]=TRiP.HMS02737}attP40/+; Tub-FRT-Gal80-FRT-Gal4, UAS-mRFP/P{GD15092}v39137*
	G	*Control*	*hs-flp ;; Tub-FRT-Gal80-FRT-Gal4, UAS-mRFP/+*
	H	*dnk KD-1*	*hs-flp ;; Tub-FRT-Gal80-FRT-Gal4, UAS-mRFP/P{GD15092}v39137*
	I, J	*RnrL KD-2*	*hs-flp ; P{y[+t7.7] v[+t1.8]=TRiP.HMS02737}attP40/+; Tub-FRT-Gal80-FRT-Gal4, UAS-mRFP/+*
	K, L	*RnrL KD-2 ; dnk KD-1*	*hs-flp ; P{y[+t7.7] v[+t1.8]=TRiP.HMS02737}attP40/+; Tub-FRT-Gal80-FRT-Gal4, UAS-mRFP/P{GD15092}v39137*
s4	A-E	RnrL KD-2	hs-flp ; P{y[+t7.7] v[+t1.8]=TRiP.HMS02737}attP40/+; Tub-FRT-Gal80-FRT-Gal4, UAS-mRFP/+
	F	Control	hs-flp ;; Tub-FRT-Gal80-FRT-Gal4, UAS-mRFP/+
	G	Control	w[*] ; P[En-Gal4], P[UAS-GFP]/+
	H	RnrL KD-2	; P[En-Gal4], P[UAS-GFP]/+ ; P{y[+t7.7] v[+t1.8]=TRiP.HMC02351}attP2/+
s5	B	Control	w[*] ; P[En-Gal4], P[UAS-GFP]/+
	C	Inx2 KD	w[*] ; P[En-Gal4], P[UAS-GFP]/+ ; UAS-Inx2 RNAi TRIP JF02446/+
	D	Control	hs-flp ;; Tub-FRT-Gal80-FRT-Gal4, UAS-mRFP/+
		Inx2 KD	hs-flp ;; Tub-FRT-Gal80-FRT-Gal4, UAS-mRFP/UAS-Inx2 RNAi TRIP JF02446
		RnrL KD-2	hs-flp ; P{y[+t7.7] v[+t1.8]=TRiP.HMS02737}attP40/+; Tub-FRT-Gal80-FRT-Gal4, UAS-mRFP/+
		RnrL KD-2 ; Inx2 KD	hs-flp ; P{y[+t7.7] v[+t1.8]=TRiP.HMS02737}attP40/+; Tub-FRT-Gal80-FRT-Gal4, UAS-mRFP/UAS-Inx2 RNAi TRIP JF02446
	B, C	NA	w[*] ; P{w[+mC]=UAS-2xEGFP}AH2/+ ; P[Delta-Gal4], tub-gal80ts/+

s6	E	NA	w[1118]
	F, G	NA	w[*] ; P{w[+mC]=UAS-2xEGFP}AH2/+ ; P[Delta-Gal4], tub-gal80ts/+
	H	Control	yw [hs-Flp]1.22 P[Tub-FRT-Gal4] P[UAS-nlsGFP]/(FM6) ; P{tubP-GAL80}LL10 P{neoFRT}40A/{neoFRT}40A [mw]
	I	Inx2 KD	yw [hs-Flp]1.22 P[Tub-FRT-Gal4] P[UAS-nlsGFP]/(FM6) ; P{tubP-GAL80}LL10 P{neoFRT}40A/{neoFRT}40A [mw] ; UAS-Inx2 RNAi TRIP JF02446/+
	J	Inx2A mutant	p{ry[+] neoFR}19A, P{w[+] tubP-GAL80}L1, P{ry[+] hsFLP}1, w/y[1] w[*] Inx2[A] P{ry[+t7.2]=neoFRT}19A ; P{w[+] UAS-CD8:GFP}LL5/+ ; P{w[+] tubP-GAL4}LL7/+
	K, L	NA	w[*] ; P{w[+mC]=UAS-2xEGFP}AH2/+ ; P[Delta-Gal4], tub-gal80ts/+
	M, O	NA	;Su(H)GBE-LacZ
s7	A-H	NA	w[1118]
s8	A	WT/WT	P{w[+mC]=Ubi-mRFP.nls}1, w[*], P{ry[+t7.2]=hsFLP}12 P{ry[+t7.2]=neoFRT}19A/P{w[+mC]=tubP-GAL80}LL1 y[1] w[*] P{ry[+t7.2]=neoFRT}19A ; P{w[+mC]=Act5C-GAL4}25FO1, P{w[+mC]=UAS-GFP.U}2/+
	B	WT/Inx2A mutant	P{w[+mC]=Ubi-mRFP.nls}1, w[*], P{ry[+t7.2]=hsFLP}12 P{ry[+t7.2]=neoFRT}19A/P{w[+mC]=tubP-GAL80}LL1 y[1] w[*] Inx2[A] P{ry[+t7.2]=neoFRT}19A ; P{w[+mC]=Act5C-GAL4}25FO1, P{w[+mC]=UAS-GFP.U}2/+
	C, D	RnrL KD-1/WT	P{w[+mC]=Ubi-mRFP.nls}1, w[*], P{ry[+t7.2]=hsFLP}12 P{ry[+t7.2]=neoFRT}19A/P{w[+mC]=tubP-GAL80}LL1 y[1] w[*] P{ry[+t7.2]=neoFRT}19A ; P{w[+mC]=Act5C-GAL4}25FO1, P{w[+mC]=UAS-GFP.U}2/+ ; P{y[+t7.7] v[+t1.8]=TRiP.HMC02351}attP2/+
	E-H	RnrL KD-1/Inx2A mutant	P{w[+mC]=Ubi-mRFP.nls}1, w[*], P{ry[+t7.2]=hsFLP}12 P{ry[+t7.2]=neoFRT}19A/P{w[+mC]=tubP-GAL80}LL1 y[1] w[*] Inx2[A] P{ry[+t7.2]=neoFRT}19A ; P{w[+mC]=Act5C-GAL4}25FO1, P{w[+mC]=UAS-GFP.U}2/P{y[+t7.7] v[+t1.8]=TRiP.HMC02351}attP2/+
s9	B, C	Control	w[*] ; P[En-Gal4], P[UAS-GFP]/+
		RFP-Inx2DN	w[*] ; P[En-Gal4], P[UAS-GFP]/pTRW-inx2 UAS-RFP-inx2 (RI1)
		CTPsyn KD-2	w[*] ; P[En-Gal4], P[UAS-GFP]/+ ; P{y[+t7.7] v[+t1.8]=TRiP.HM04062}attP2/+
		RFP-Inx2DN ; CTPsyn KD-2	w[*] ; P[En-Gal4], P[UAS-GFP]/pTRW-inx2 UAS-RFP-inx2 (RI1); P{y[+t7.7] v[+t1.8]=TRiP.HM04062}attP2/+
		CTPsyn KD-3	w[*] ; P[En-Gal4], P[UAS-GFP]/+ ; P{y[+t7.7] v[+t1.8]=TRiP.JF02214}attP2/+
		RFP-Inx2DN ; CTPsyn KD-3	w[*] ; P[En-Gal4], P[UAS-GFP]/pTRW-inx2 UAS-RFP-inx2 (RI1) ; P{y[+t7.7] v[+t1.8]=TRiP.JF02214}attP2/+
		bur KD-2	w[*] ; P[En-Gal4], P[UAS-GFP]/+ ; P{y[+t7.7] v[+t1.8]=TRiP.JF01503}attP2/+
		RFP-Inx2DN ; bur KD-2	w[*] ; P[En-Gal4], P[UAS-GFP]/pTRW-inx2 UAS-RFP-inx2 (RI1) ; P{y[+t7.7] v[+t1.8]=TRiP.JF01503}attP2/+
		Prps KD-2	w[*] ; P[En-Gal4], P[UAS-GFP]/+ ; P{y[+t7.7] v[+t1.8]=TRiP.GL00463}attP2/+
		RFP-Inx2DN ; Prps KD-2	w[*] ; P[En-Gal4], P[UAS-GFP]/pTRW-inx2 UAS-RFP-inx2 (RI1) ; P{y[+t7.7] v[+t1.8]=TRiP.GL00463}attP2/+
	D	dnk KD-1	w[*] ; P[En-Gal4], P[UAS-GFP]/+ ; P{GD15092}v39137/+
	E-G	RFP-Inx2DN ; dnk KD-1	w[*] ; P[En-Gal4], P[UAS-GFP]/pTRW-inx2 UAS-RFP-inx2 (RI1) ; P{GD15092}v39137/+

Table S3. List of antibodies.

Antibody	Host	Source (Reference)	Dilution used
GFP	Chicken	Invitrogen A10262	1:2000
RFP	Mouse	Invitrogen (RF5R)	1:2000
RFP	Rabbit	Takara Living Colors 632496	1:1000
γH2Av	Rabbit	Rockland 600-401-914	1:2000
γH2Av	Mouse	DSHB UNC93-5.2.1	1:200
RnrL	Rabbit	Arnaoutov et al., 2020 (A. Arnaoutov)	1:200 (gut), 1:100 (disc)
DNK	Rabbit	Knecht et al., 2000 (A. Lalouette)	1:20000
Armadillo	Mouse	DSHB N2 7A1	1:200
Delta	Mouse	DSHB C594.9ba	1:1000
Prospero	Mouse	DSHB MR1A-c	1:2000
Bgal	Goat	Biogenesis 466-1409	1:200
Bgal	Chicken	Abcam ab9361	1:2000
Inx2	Rabbit	Ammer et al., 2022 (G. Ammer)	1:1000
Inx2	Guinea Pig	Smendziuk et al., 2015 (G. Tanentzapf)	1:500
Inx7	Rabbit	Ostrowski et al., 2008 (R. Bauer)	1:100
Inx3	Rabbit	Bohrmann & Zimmermann, 2008 (R. Bauer)	1:70
Coracle	Mouse	DSHB C615.16	1:100
pH3	Rabbit	Merck Millipore 06-570	1:2000
anti-Chicken DyLight-488	Donkey	Jackson 703-486-155	1:2000
anti-Goat DyLight-488	Donkey	Jackson 705-486-147	1:2000
anti-Guinea Pig DyLight-549	Donkey	Jackson 706-506-148	1:2000
anti-Guinea Pig DyLight-649	Donkey	Jackson 706-496-148	1:2000
anti-Mouse DyLight-488	Donkey	Jackson 715-486-150	1:2000
anti-Mouse DyLight-549	Donkey	Jackson 715-506-150	1:2000
anti-Mouse DyLight-649	Donkey	Jackson 715-496-150	1:2000
anti-Rabbit DyLight-488	Donkey	Jackson 711-486-152	1:2000
anti-Rabbit DyLight-549	Donkey	Jackson 711-506-152	1:2000
anti-Rabbit DyLight-649	Donkey	Jackson 711-496-152	1:2000